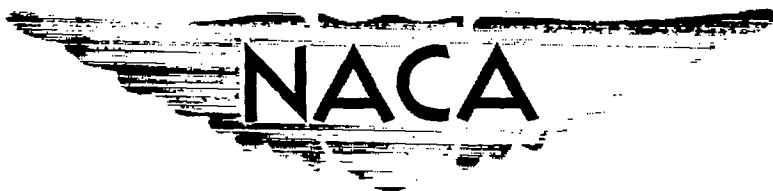


~~CONFIDENTIAL~~

Reg 6236

Copy 209  
RM E55F27

NACA RM E55F27



AUG 12 1955

TECH LIBRARY KAFB, NM

0144052

# RESEARCH MEMORANDUM

FREE-FLIGHT HEAT-TRANSFER MEASUREMENTS ON TWO  
20°-CONE-CYLINDERS AT MACH NUMBERS

FROM 1.3 TO 4.9

By Leonard Rabb and Scott H. Simpkinson

Lewis Flight Propulsion Laboratory  
Cleveland, Ohio

CLASSIFIED DOCUMENT

This material contains information affecting the National Defense of the United States within the meaning of the espionage laws, Title 18, U.S.C., Secs. 793 and 794, the transmission or revelation of which in any manner to an unauthorized person is prohibited by law.

## NATIONAL ADVISORY COMMITTEE FOR AERONAUTICS

WASHINGTON  
July 18, 1955

~~CONFIDENTIAL~~

~~CONFIDENTIAL~~

6925



## NATIONAL ADVISORY COMMITTEE FOR AERONAUTICS

RESEARCH MEMORANDUM

## FREE-FLIGHT HEAT-TRANSFER MEASUREMENTS ON TWO 20°-CONE-CYLINDERS

AT MACH NUMBERS FROM 1.3 TO 4.9

By Leonard Rabb and Scott H. Simpkinson

## SUMMARY

Heat-transfer data were obtained in free flight at supersonic Mach numbers up to 4.90 and local Reynolds numbers per foot up to 27.7 million. Two 20°-included-angle cone-cylinder models, instrumented along the internal surface of the cone, were launched from a carrier airplane at an altitude of approximately 36,000 feet. Each model was accelerated to maximum velocity by an internally housed rocket. The models followed zero-lift trajectories until ground impact.

Boundary-layer transition was indicated on one model at various stations along the cone. For this model, transition occurred at each station at a constant surface Reynolds number of 8.0 million and a ratio of skin temperature to local stream temperature of 1.0. Both models had turbulent boundary layers in the region where, according to Van Driest's predictions, laminar boundary layers should have existed. However, a surface discontinuity may have induced turbulent flow.

The maximum deviation between the local turbulent Stanton numbers predicted by Van Driest and the observed data was 20 percent when the Reynolds number was based on the distance to the cone apex. The drag coefficient was 0.22 at a free-stream Mach number of 4.69.

## INTRODUCTION

The design of supersonic missiles requires an understanding of laminar and turbulent boundary-layer characteristics under various conditions of heat transfer. Many theoretical analyses of the laminar boundary layer and, to a lesser extent, of the turbulent boundary layer, have been made. Attempts have also been made to gain an understanding of the phenomenon of "boundary-layer transition." However, the factors affecting the transition from a laminar to a turbulent boundary layer and the characteristics of the turbulent boundary layer itself have not been adequately evaluated. Experimental data on the subject are particularly needed at

high Reynolds numbers and at very low turbulence conditions. Since these conditions are difficult to obtain in wind tunnels, the NACA has implemented its over-all program with a series of free-flight tests at Wallops Island, Virginia.

The data reported herein were obtained from two test models designed and constructed at the NACA Lewis laboratory. The test models (fig. 1) were 20°-included-angle cone-cylinder bodies of revolution, which were launched subsonically at an altitude of approximately 36,000 feet. An internally housed rocket accelerated the test models to maximum velocities. Following the rocket-powered period, the models decelerated because of drag forces. The cone-cylinders were fin-stabilized and followed zero-lift trajectories until ground impact.

Each model was instrumented primarily to obtain the time history of the skin temperature along the cone, and the data were obtained with a 10-channel telemetering unit.

#### APPARATUS AND PROCEDURE

The two models reported herein are designated model 3 and model 4. Each model was approximately 80 inches long and consisted basically of a 20°-included-angle cone with a 9.25-inch-diameter cylindrical afterbody. The general dimensions and specifications for the models are given in figure 1. Solid-propellant rockets were used to accelerate the models to peak velocity. The rockets were maintained at 100° F before ignition. Both models were stabilized by a cruciform fin arrangement. The fins were fabricated of 11-gage (0.125-in.) carbon steel and had a root-chord thickness ratio of 0.011. The leading and trailing edges of the fins were beveled. Lead ballast (13.5 lb) was used in the nose to provide stability at the peak Mach numbers. The shells of the models were seam-welded Inconel and were hand-polished to a smooth mirror finish.

The models were fabricated in three sections, as shown by figure 2. The forward section served as a radio-telemeter antenna and was separated from the intermediate section by a ceramic ring. This ring caused a surface discontinuity that varied circumferentially from a bump to a depression. The maximum height of this surface irregularity was approximately 0.003 inch. The use of surface putty on model 4 did not entirely eliminate the roughness. Surface putty was not used on model 3.

The following instrumentation was used for each of the two models:

- (1) One linear accelerometer (for axial accelerations)
- (2) One flush static-pressure orifice on aft part of cylinder (fig. 1)

- (3) One total-pressure probe (fig. 1)
- (4) Seven resistance-wire temperature elements located along inside surface of intermediate section (fig. 3)

The temperature-sensitive resistance elements (fig. 4) consisted of fine platinum wires approximately  $4\frac{1}{2}$  inches long. Two inches at each end were plated with silver to form low-resistance lead wires, leaving the  $\frac{1}{2}$  inch at the center as the effective sensing element. The wires were cemented to the skin with a layer of high-temperature insulating varnish that was only a few thousandths of an inch thick. The entire installation was roughly 0.004 inch thick. Special junction blocks located 3 inches from the sensing elements were used to join the silvered lead wires to the coaxial cables from the telemeter units.

The models were carried aloft by an F-82 airplane and were released at an altitude of approximately 36,000 feet. Data were radio-telemetered to the ground receiving stations from the 10-channel telemeter unit in the intermediate section. Additional data were obtained for model 4 by an SCR-584 radar unit. The radar was equipped with optical as well as automatic tracking facilities. No radar data were obtained for model 3.

The time constant of the temperature elements was less than 0.003 second. This resulted in a maximum error of  $1^{\circ}$  R in the measured skin temperature  $t_s$  and  $0.3^{\circ}$  R per second in the rate of change of the skin temperature  $dt_s/d\tau$ . (Symbols are defined in appendix A.) These errors are systematic errors that directly affect the calculated heat-transfer coefficients  $h_{cv}$ . Additional systematic errors in  $h_{cv}$  were caused by radiation heat losses and by a temperature drop through the skin to the internal surface where the elements were located. The calculated values of  $h_{cv}$  that are discussed in this report are uncorrected for these systematic errors and therefore are low by a maximum of 5 percent.

Random errors also influenced the heat-transfer coefficient  $h_{cv}$ . The probable error due to these random errors varied from  $\pm 4$  to  $\pm 6$  percent during the acceleration phase of the flights. These errors are in addition to the above-mentioned systematic errors.

## RESULTS AND DISCUSSION

Both test models were launched at free-stream Mach numbers of 0.55 and followed zero-lift trajectories until impact. The rocket motors fired after delay times of 19.8 and 5.4 seconds, respectively, for models 3 and 4. The shorter delay time of model 4 prevented it from pitching downward. A flatter trajectory resulted (fig. 5), which increased the

flight time from 31.0 seconds for model 3 to 55.0 seconds for model 4. (For convenience in presenting the data, the time histories are shown from 19 to 31 seconds for model 3 and from 4 to 36 seconds for model 4.)

The maximum free-stream Mach numbers attained were 4.42 (model 3) and 4.90 (model 4). Visual contact with model 4 was lost immediately after rocket burn-out, and the subsequent radar data were obtained from the automatic tracking facilities of the SCR-584 radar unit.

The telemeter signal of model 3 was intermittent. This intermittency, however, did not reflect on the accuracy of the recorded data, because the intermittency was in the carrier signal and not in the sub-carrier data channels. The telemeter signal for model 4 was continuous throughout the entire flight. Of a total of 20 channels telemetered for the two models, three of the temperature channels did not function properly. No data are presented for these channels.

#### Primary Data

Free-stream conditions. - The time histories of the measured static pressures on the cylindrical afterbodies of models 3 and 4 are presented in figure 6. The measured pressures were less than free-stream static pressures because of the flow expansion at the cone-cylinder shoulder. Corrections (ref. 1) were applied to the measured static pressures to obtain the free-stream static pressures  $p_0$ . The corrected values of  $p_0$  are shown in figure 6 as solid lines. The free-stream static pressures of model 4 were also obtained from radar data (see appendix B). Figure 6(b) shows the close agreement of the radar data and the corrected values of  $p_0$ .

The time histories of the measured total pressures for the two models are shown in figure 7. The values do not represent free-stream values of total pressure because of the inherent normal-shock loss of the probe and the slight loss in total pressure across the conical shock wave originating at the cone apex.

The free-stream Mach number, velocity, and Reynolds number per foot are presented in figures 8, 9, and 10, respectively. The free-stream Mach numbers of model 3 (fig. 8(a)) increased from approximately 0.8 at rocket ignition to a maximum of 4.42. Model 4 (fig. 8(b)) reached a maximum free-stream Mach number of 4.90. Because of the long rocket ignition-delay time (mentioned previously) and the resulting loss in altitude, model 3 was still at a supersonic Mach number (2.42) at impact. Model 4 decelerated to a subsonic Mach number of 0.80 at impact. The maximum free-stream velocities attained were 4720 and 5080 feet per second for models 3 and 4, respectively (fig. 9). The maximum free-stream Reynolds numbers per foot ( $Re_0/ft$ ) were 20.8 million and 11.6 million (fig. 10).

Figure 10 also presents the local cone surface Reynolds numbers per foot ( $Re_{\delta}/ft$ ), which are appreciably higher than the corresponding free-stream values. The maximum cone Reynolds numbers per foot were 27.7 million and 16.6 million for models 3 and 4, respectively.

Axial acceleration. - The axial-acceleration measurements (excluding gravity) are presented in figure 11 in terms of gravitational units (g's). The acceleration data for model 3 were not continuous throughout the flight but do present an adequate time history after 22.75 seconds. The peak acceleration which should occur immediately after rocket ignition was not recorded for model 3. The highest recorded value was 27.3 g's at 24.1 seconds (fig. 11(a)). The peak acceleration of model 4 was observed immediately following rocket ignition (fig. 11(b)) to be 50.84 g's. A second peak of 28.4 g's occurred at 9.6 seconds. The acceleration time history of model 4 corresponds closely with the anticipated rocket thrust time history.

Following the power-on phase, the acceleration (excluding gravity) was influenced only by the drag forces acting on the models. The total drag coefficient was therefore based on the accelerometer measurements during the decelerating phase for both models. The total drag coefficient  $C_D$ , based on a maximum cross-sectional area of 0.466 square foot, is presented in figure 12 for models 3 and 4. The drag coefficient increased from 0.16 at a free-stream Mach number of 0.80 to 0.55 at  $M_0$  of 0.99 and then decreased to 0.22 at  $M_0$  of 4.69.

Skin temperatures. - The time histories of the measured skin temperatures  $t_s$  are shown in figures 13 and 14. Also shown in each figure are the free-stream total temperature  $T_0$ , the theoretical insulated skin temperature  $t_{ad}$  based on an assumed recovery factor (see appendix B), the static temperature just outside the conical boundary layer  $t_{\delta}$ , and the free-stream static temperature  $t_0$ .

The peak skin temperatures of the rear five measurements on model 3 agreed quite well with the theoretical adiabatic wall temperature at the corresponding times. However, this fact cannot be used to verify the theoretical recovery factor. To do so would require a precise knowledge of the emissivity of the skin. Other factors, such as the rapid change of  $T_0$  with time, also make the determination of the recovery factor difficult. The data of the most forward element show the peak skin temperature to be considerably lower than the corresponding  $t_{ad}$ . Calculations indicate that this difference could be due to heat flow to the structural bulkhead close to the most forward temperature element (fig. 3(a)).

The data for the rear three temperature elements of model 4 also show good agreement between the peak skin temperature and the theoretical insulated skin temperature. However, the peak skin temperatures presented for the two most forward elements (located 180° apart) do not correspond to  $t_{ad}$  (fig. 14). This difference is not believed to be due to a "bulkhead effect," since calculations indicate negligible "bulkhead effect" for these elements. The reasons for the low values of the peak skin temperatures for the forward elements are not clearly understood.

The skin temperatures presented in figures 13 and 14 exceed the free-stream total temperatures during the latter portion of the flight because of the heat capacity of the metal skin. A maximum skin temperature of 1650° R was observed on model 3 at a slant distance  $l$  from the cone apex of 24.21 inches. The peak skin temperature of model 4 was 1565° R at  $l = 17.23$  inches. The following table presents the maximum observed temperature and maximum rate of rise for each temperature measuring station:

Model 3			Model 4		
Slant distance to apex, $l$ , in.	Maximum temperature, $t_s$ , °R	Maximum rate of temperature rise, °R/sec	Slant distance to apex, $l$ , in.	Maximum temperature, $t_s$ , °R	Maximum rate of temperature rise, °R/sec
14.46	1510	330	15.29	1435	265
18.40	1580	320	15.23	1435	290
20.34	1575	290	17.23	1565	270
22.34	1500	280	21.10	1460	240
24.21	1650	320	22.91	1450	265
25.96	1510	290			

The peak temperatures of models 3 and 4 do not show a smooth axial variation. The high-peak temperature of 1650° R for model 3 at  $l = 24.21$  appears out of place, as does the peak temperature of 1565° R at  $l = 17.23$  for model 4. These irregularities are not fully understood. The authors feel, however, that they are not instrumentation errors.

The higher values of peak skin temperatures and rates of temperature rise for model 3 as compared with model 4 were the result of the flight trajectories. Model 3 was at lower altitudes (higher air density) than model 4 at comparable flight speeds.

The maximum rate of skin-temperature rise observed was 330° R per second at  $l = 14.46$  inches for model 3. This value corresponds to a heat-transfer rate of 0.35 Btu/(sq in.)(sec).

## Heat-Transfer Results

Experimental Stanton number. - The time histories of the measured skin temperatures were used to compute heat-transfer coefficients as described in appendix B. Figure 15 shows these coefficients for model 3 in the nondimensional form of Stanton number  $St$  plotted for free-stream Mach numbers of 2.71 to 4.42. Corresponding cone Reynolds numbers per foot of 10.3 million to 27.2 million are also indicated along the abscissa. In addition, the figure includes the ratio of the measured skin temperature  $t_s$  to the calculated static temperature just outside the boundary layer  $t_\delta$ . Values of this ratio vary from 1.2 to 2.2. Results indicate that, throughout the Mach number range shown, the boundary layer of model 3 was turbulent all along the instrumented portion of the cone.

Figure 15 also includes the theoretical curves of Stanton number as predicted by Van Driest in reference 2 and as corrected to cone values (ref. 3). Two characteristic lengths were used to compute the Reynolds number and therefore show the effect on Stanton number of the movement of the effective origin of transition. One computation was made with  $l$  (the distance of the temperature element from the cone apex) and the other with  $l_1$  (the distance between the element and the junction of the antenna and the ceramic spacer ring).

The data of model 4 are presented in figure 16 for free-stream Mach numbers from 1.31 to 4.90. Corresponding cone Reynolds numbers per foot and temperature ratios  $t_s/t_\delta$  varied from 3.0 million to 16.7 million and 1.0 to 2.0, respectively. The theoretical Stanton numbers in figure 16 were based on Reynolds numbers from the cone apex. Predicted laminar values of Stanton number are also shown in figure 16 (ref. 4).

The maximum difference between the experimental Stanton numbers and the values of Van Driest for both models is 20 percent when the local Reynolds number is based on the length to the cone apex  $l$ .

The data presented in figures 15 and 16 are only for the accelerating portion of the flights.<sup>1</sup>

<sup>1</sup>As mentioned in appendix B, the experimental Stanton number is related to the specific heat of the skin. This in turn is a function of the skin temperature. Data obtained from reference 5 show a sharp discontinuity in the curve of instantaneous specific heat against temperature for Inconel at temperatures between 1390° and 1490° R. Consequently, the Stanton number cannot be evaluated accurately through this temperature range. Also, the error in Stanton number approaches infinity as the slopes of the skin-temperature curves approach zero. Additional inaccuracies occur when the difference between  $t_{ad}$  and  $t_s$  becomes small. These factors affect the calculations during the decelerating phase of the flights.

Boundary-layer transition. - The data for model 4 (figs. 14 and 16) clearly indicate the boundary-layer transition from laminar to turbulent flow. Boundary-layer transition is characterized by large changes in the Stanton number, as shown in figure 16. For example, in figure 16(c), the Stanton number increases from 0.00032 at  $M_0 = 2.39$  to 0.00119 at  $M_0 = 2.51$ . The associated rapid rise in skin temperatures at approximately 8 seconds is shown in figure 14(c). The skin temperatures from 6 to 10 seconds of figure 14 are presented in figure 17 on expanded scales. The approximate time of transition at each temperature station is also indicated.

Transition for model 4 first occurred at approximately 7 seconds at  $\gamma = 22.91$ . The transition point then moved forward until at 8.0 seconds the entire boundary layer over the instrumented section of the cone was turbulent. The movement of the transition point is also illustrated in the top part of figure 18, which presents the free-stream Mach number at the time of transition for each station. Transition occurred at approximate Mach numbers of 1.85 for the rear stations and 2.50 for the forward stations. The cone surface Reynolds number at transition was approximately constant at 8.0 million for each station (lower part of fig. 18). The transition Reynolds number may have been influenced by the surface discontinuity at the antenna junction.

Boundary-layer stability. - According to Lees (ref. 6) and Van Driest (ref. 7), complete stabilization of a laminar boundary layer is possible under certain conditions. Some of the data of this report are compared with the stability criteria of Van Driest (ref. 7) in figure 19. The theoretical stability curve is plotted for infinite Reynolds number and a Prandtl number of 0.75 with the viscosity based on the Sutherland equation. This shows that for a given local Mach number  $M_0$ , values of  $t_s/t_0$  equal to or less than those given by Van Driest would be sufficient to provide complete stabilization of the laminar boundary layer. Some experimental data of references 8 and 9 tend to confirm the predictions of references 6 and 7. However, typical data of this report, presented in figure 19, show turbulent boundary layers well within the area of complete boundary-layer stabilization predicted by Van Driest.

The data of model 4 at  $\gamma = 15.29$  also show a transition point at  $t_s/t_0 = 1.0$  and a cone surface Mach number  $M_0$  of 2.29. If transition occurred along the instrumented portion of the cone of model 3, it occurred very early in the flight where skin-temperature data were not recorded because of the intermittent telemeter signal previously mentioned.

The fact that turbulent boundary layers and a transition point were indicated in a region of predicted infinite stability may be due to the surface roughness at the antenna junction, although an attempt was made to remove the roughness of model 4.

## SUMMARY OF RESULTS

Two 20°-cone-cylinder bodies of revolution were instrumented to obtain heat-transfer data in free-flight. The data were obtained at free-stream Mach numbers up to 4.90 and at Reynolds numbers per foot up to 27.7 million, with the following results:

1. Transition was indicated at several stations on one model at a constant cone surface Reynolds number of 8.0 million and a ratio of skin temperature to local stream temperature of 1.0.
2. Turbulent flow occurred on both test models in the region of complete boundary-layer stabilization predicted by Van Driest. However, a surface discontinuity may have induced transition.
3. The local turbulent heat-transfer coefficient differed from the theoretical values of Van Driest by a maximum of 20 percent, when the cone Reynolds number was based on the distance from the cone apex.
4. A maximum skin temperature of 1650° R and a maximum rate of temperature rise of 330° R per second were recorded.
5. The drag coefficient of the test models varied from 0.55 at a free-stream Mach number of 0.99 to 0.22 at a free-stream Mach number of 4.69.

Lewis Flight Propulsion Laboratory  
National Advisory Committee for Aeronautics  
Cleveland, Ohio, April 27, 1955

~~CONFIDENTIAL~~

## APPENDIX A

## SYMBOLS

The following symbols are used in this report:

A	maximum cross-sectional area, 0.466 sq ft
a	axial acceleration, g's (exclusive of gravity)
$C_D$	total drag coefficient
$c_p$	specific heat of air at constant pressure, Btu/(slug)(°R)
$c_s$	specific heat of skin, Btu/(lb)(°R)
G	heat capacity of skin, $(c_s)(x)(W_s)$ , Btu/(sq ft)(°R)
g	acceleration due to gravity, 32.17 ft/sec <sup>2</sup>
$H_{st}$	static enthalpy, Btu/lb
$H_{tot}$	total enthalpy, Btu/lb
$h_{cv}$	local convective heat-transfer coefficient, $G(dt_s/d\tau)/(t_{ad} - t_s)$ , Btu/(sec)(sq ft)(°R)
k	thermal conductivity, Btu/(sec)(ft)(°R)
l	slant distance from cone apex, in.
M	Mach number
Nu	Nusselt number, $h_{cv}l/k$
P	total pressure, lb/sq ft
Pr	Prandtl number, $c_p\mu/k$
p	static pressure, lb/sq ft
q	heat transferred per second, Btu/sec
R	gas constant, 53.3 ft-lb/(lb)(°R)

3661

~~CONFIDENTIAL~~

- 19661
- CF-2 back
- Re Reynolds number,  $Vl\rho/12\mu$
- $S_w$  wetted surface area
- St Stanton number,  $h_{cv}/c_p\rho\delta V_\delta$
- T total temperature,  $^{\circ}R$
- t static temperature,  $^{\circ}R$
- V velocity, ft/sec
- W weight of test model at rocket burn-out
- $W_s$  specific weight of Inconel skin, 530.5 lb/cu ft at  $70^{\circ} F$
- x skin thickness, ft
- $\beta$  recovery factor ( $Pr^{1/3}$  for turbulent flow;  $Pr^{1/2}$  for laminar flow)
- $\gamma$  ratio of specific heat of air at constant pressure to specific heat of air at constant volume
- $\mu$  coefficient of viscosity of air, lb-sec/sq ft
- $\rho$  density of air, slugs/cu ft
- $\tau$  time, sec
- $\psi$  angle between flight path and vertical reference line in space
- Subscripts:
- ad adiabatic wall
- i initial
- m measured
- s skin
- $\delta$  conditions just outside conical boundary layer
- $\sigma$  behind normal shock
- O free stream
- l slant distance from temperature element to junction of antenna and ceramic insulator ring

## APPENDIX B

## METHOD OF CALCULATION

The free-stream static pressure  $p_0$  encountered by the test models was obtained from the flush orifice located on the cylindrical afterbody. These measurements were corrected for the flow expansion around the cone-cylinder shoulder in accordance with reference 1. The ambient pressure was also obtained from the radar data as follows. The SCR-584 radar tracking unit observed the carrier plane as it descended. At specified intervals of pressure altitude, the radar recorded the position of the airplane. From such a survey, a curve of static pressure against altitude could be obtained. The radar also provided a time history of the altitude encountered by the test models. By combining the curves of  $p_0$  against altitude and altitude against time, the curve of  $p_0$  against time was obtained. The free-stream static temperature was obtained from a calibrated temperature probe at each pressure altitude as the carrier airplane descended.

The free-stream velocity  $V_0$  was calculated by summing the incremental changes of velocity over short time intervals. The following equation was used:

$$V_0 = V_1 + 32.17 \int_{\tau_1}^{\tau_2} (\bar{a} + \cos \bar{\psi}) \Delta \tau \quad (B1)$$

where

$\bar{a}$  average axial acceleration, g's (exclusive of gravity), during time interval  $\Delta \tau$

$\bar{\psi}$  average angle between flight path and vertical reference line in space during time interval  $\Delta \tau$

The velocity was also obtained from

$$V_0 = M_0 \sqrt{\gamma g R t_0} \quad (B2)$$

where  $M_0$  was calculated from the Rayleigh equation:

$$\frac{P_0}{P_{0,\sigma}} = \frac{\left(\frac{2\gamma}{\gamma+1} M_0^2 - \frac{\gamma-1}{\gamma+1}\right)^{\frac{1}{\gamma-1}}}{\left(\frac{\gamma+1}{2} M_0^2\right)^{\frac{\gamma}{\gamma-1}}} \quad (B3)$$

and  $P_{0,\sigma}$  is the measured total pressure behind the normal shock corrected for total-pressure loss across oblique shock wave at apex of cone. The free-stream velocity  $V_0$  was also obtained directly from the radar data.

The total drag coefficient was calculated for the decelerating portion of the flight from

$$C_D = \frac{2W a}{\gamma P_0 M_0^2 A} \quad (B4)$$

where  $W$  is the weight of the test model at rocket burn-out.

The free-stream total temperature  $T_0$  was obtained by evaluating the total enthalpy  $H_{tot,0}$  from

$$H_{tot,0} = H_{st,0} + \frac{v_0^2}{50,056} \quad (B5)$$

Reference 10 gives the corresponding  $T_0$  for the calculated  $H_{tot,0}$ .

The free-stream Reynolds number per foot  $Re_0/ft$  was calculated from

$$Re_0/ft = \frac{V_0 \rho_0}{\mu_0} \quad (B6)$$

where  $\rho_0$  was obtained from the general gas law  $\left(\rho_0 = \frac{P_0}{gRt_0}\right)$ , and  $\mu_0$  was obtained from

- (1)  $t_0$  and the Sutherland equation (model 3)
- (2)  $t_0$  and reference 10 (model 4)

The Reynolds number per foot at the cone surface  $Re_\delta/ft$  was obtained from

$$Re_{\delta}/ft = \left( \frac{V_{\delta} \rho_{\delta}}{\mu_{\delta}} \right) \quad (B7)$$

where  $V_{\delta}$ ,  $t_{\delta}$ , and  $\rho_{\delta}$  were obtained from the M.I.T. cone tables (ref. 11). The viscosity,  $\mu_{\delta}$ , was evaluated at  $t_{\delta}$  and obtained from reference 10.

The convective heat-transfer coefficient  $h_{cv}$  was obtained by writing a heat balance at the wall that neglected small radiation and conduction losses:

$$G \frac{dt_s}{d\tau} = \frac{q}{S_w} = h_{cv}(t_{ad} - t_s) \quad (B8)$$

and, therefore,

$$h_{cv} = \frac{G \frac{dt_s}{d\tau}}{t_{ad} - t_s}$$

The heat capacity of the wall is

$$G = (c_s)(x)(W_s) \quad (B9)$$

where  $c_s$  is from reference 5.

The adiabatic wall temperature  $t_{ad}$  was calculated by

$$t_{ad} = t_{\delta} + \beta(T_0 - t_{\delta}) \quad (B10)$$

where

$$\beta = Pr^{1/3} \quad \text{for turbulent flow} \quad (B11)$$

$$\beta = Pr^{1/2} \quad \text{for laminar flow} \quad (B12)$$

and the Prandtl number  $Pr$  was evaluated at  $t_{\delta}$ .

The heat-transfer coefficient was calculated in the nondimensional form as Stanton number  $St$ :

$$St = \frac{h_{cv}}{c_p \rho_{\delta} V_{\delta}} \quad (B13)$$

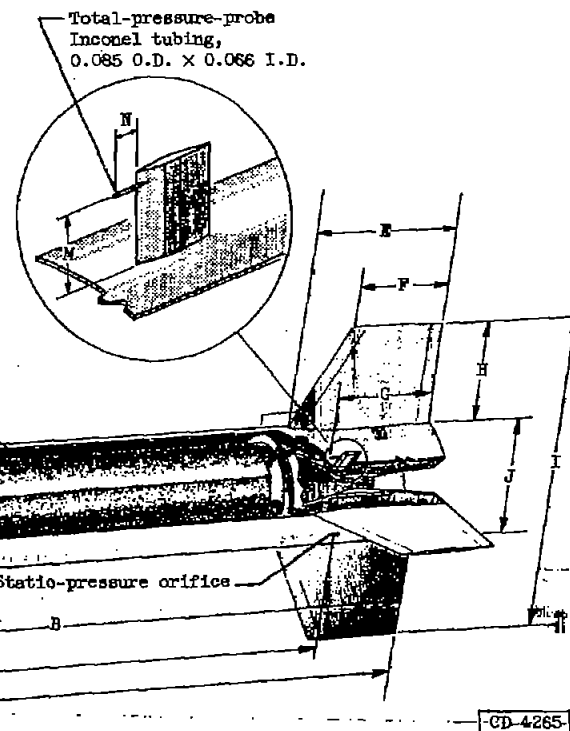
where  $c_p$  was evaluated at  $t_{\delta}$ .

## REFERENCES

1. Clippinger, R. F., Giese, J. H., and Carter, W. C.: Tables of Supersonic Flows About Cone Cylinders. Pt. I - Surface Data. Rep. No. 729, Ballistic Res. Labs., Aberdeen Proving Ground (Md.), July 1950. (Proj. TB3-0108H of Res. and Dev. Div., Ord. Dept.)
2. Van Driest, E. R.: The Turbulent Boundary Layer for Compressible Fluids on a Flat Plate with Heat Transfer. Rep. AL-997, Aerophysics Lab., North American Aviation, Inc., Jan. 27, 1950. (Proj. MX-770.)
3. Van Driest, E. R.: Turbulent Boundary Layer on a Cone in Supersonic Flow at Zero Angle of Attack. Rep. AL-1042, Aerophysics Lab., North American Aviation, Inc., Mar. 22, 1951. (Contract W33-038ac-14191, Proj. MX-770.)
4. Eckert, E. R. G.: Introduction to the Transfer of Heat and Mass. First ed., McGraw-Hill Book Co., Inc., 1950, p. 156.
5. Douglas, Thomas B., and Harman, Ann W.: The Enthalpy and Heat Capacity of Three Representative Inconel Alloys from 0° to 900° C. Rep. 3757, Thermodynamic Sec., Div. Heat and Power, Nat. Bur. Standards, Oct. 14, 1954.
6. Lees, Lester: The Stability of the Laminar Boundary Layer in a Compressible Fluid. NACA Rep. 876, 1947. (Supersedes NACA TN 1360.)
7. Van Driest, E. R.: Calculation of the Stability of the Laminar Boundary Layer in a Compressible Fluid on a Flat Plate with Heat Transfer. Jour. Aero. Sci., vol. 19, no. 12, Dec. 1952, pp. 801-812.
8. Fischer, W. W., and Norris, R. H.: Supersonic Convective Heat-Transfer Correlation from Skin-Temperature Measurements on a V-2 Rocket in Flight. Trans. A.S.M.E., vol. 71, no. 5, July 1949, pp. 457-467; discussion, pp. 467-469.
9. Sternberg, Joseph: A Free-Flight Investigation of the Possibility of High Reynolds Number Supersonic Laminar Boundary Layers. Jour. Aero. Sci., vol. 19, no. 11, Nov. 1952, pp. 721-733.
10. Keenan, Joseph H., and Kaye, Joseph: Thermodynamic Properties of Air. John Wiley & Sons, Inc., 1945.
11. The Staff of the Computing Section Center of Analysis: Tables of Supersonic Flow Around Cones. Tech. Rep. No. 1, M.I.T., 1947. (Contract NOrd 9169.)

3661

Specification	Model 3	Model 4
Gross weight at launching, lb	204	208
Weight at end of rocket boost, lb	101	105
Launching altitude, ft	38,000	37,000
Rocket ignition-delay time, sec	19.8	5.4
Design Mach number at 32,000 ft	5.0	5.0
Center of gravity at launching (station), in.	47.87	48.13
Center of gravity at end of rocket boost (station), in.	43.50	43.93
Cross-sectional area (max.), sq ft	0.466	0.466
Skin thickness at temperature measuring stations, in.	0.0270	0.0296
Skin thickness of shell, in.	0.032	0.032
Fin area (2 fins), sq in.	152	152
Model fineness ratio	8.65	8.71
Stabilizing-fin root-chord - thickness ratio	0.011	0.011



Dimensions in inches					
Dimension	Model 3	Model 4	Dimension	Model 3	Model 4
A	26.25	28.10	H	8.00	8.00
B	53.75	54.50	I	25.25	25.25
C	70.50	72.10	J	9.25	9.25
D	80.00	80.60	K	11.77	11.77
E	11.50	11.50	L	1.50	1.40
F	7.50	7.50	M	1.25	1.25
G	10.00	10.25	N	.38	.38

Figure 1. - General dimensions and specifications for models 3 and 4.

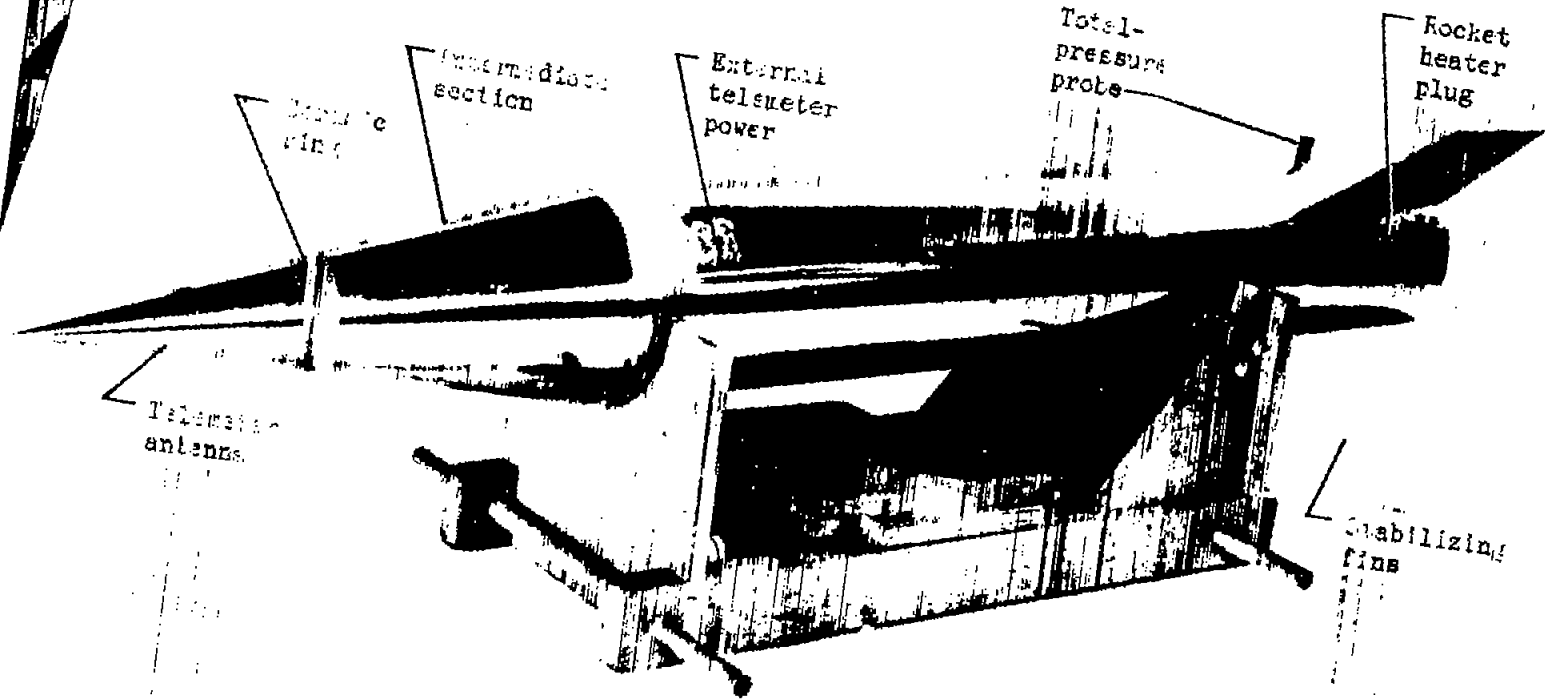
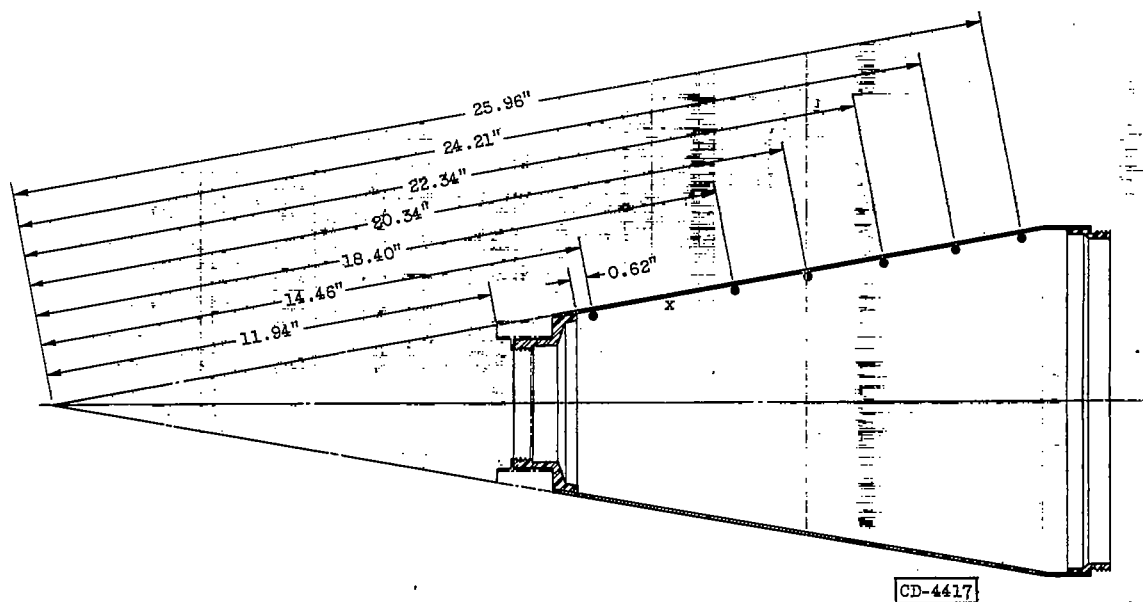
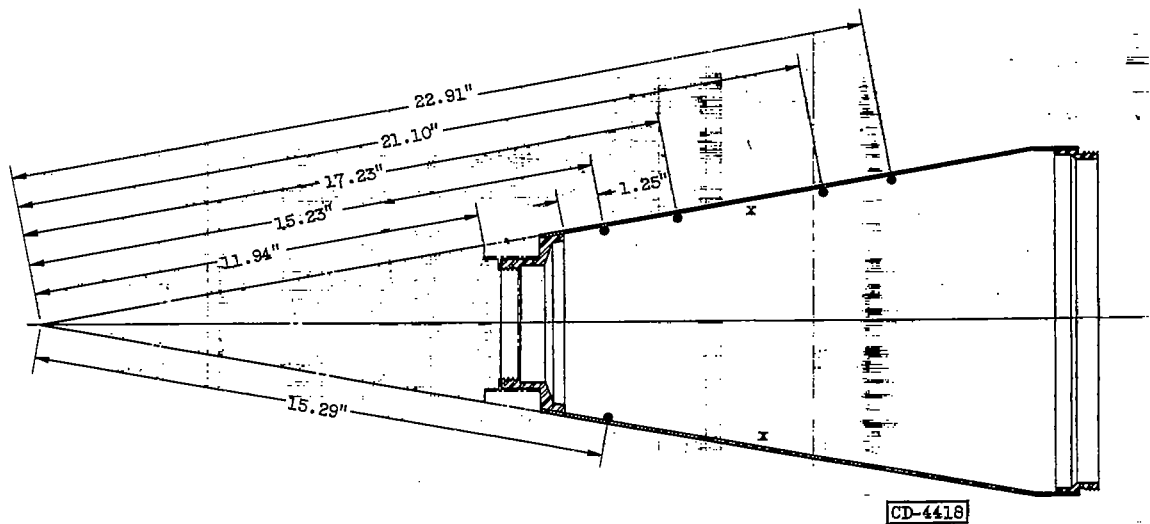


Figure 2. - Photograph of 20°-cone-cylinder test model.

C-36509



(a) Model 3.



(b) Model 4.

Figure 3. - Location of resistance-wire temperature elements. (Data not recorded from elements x.)

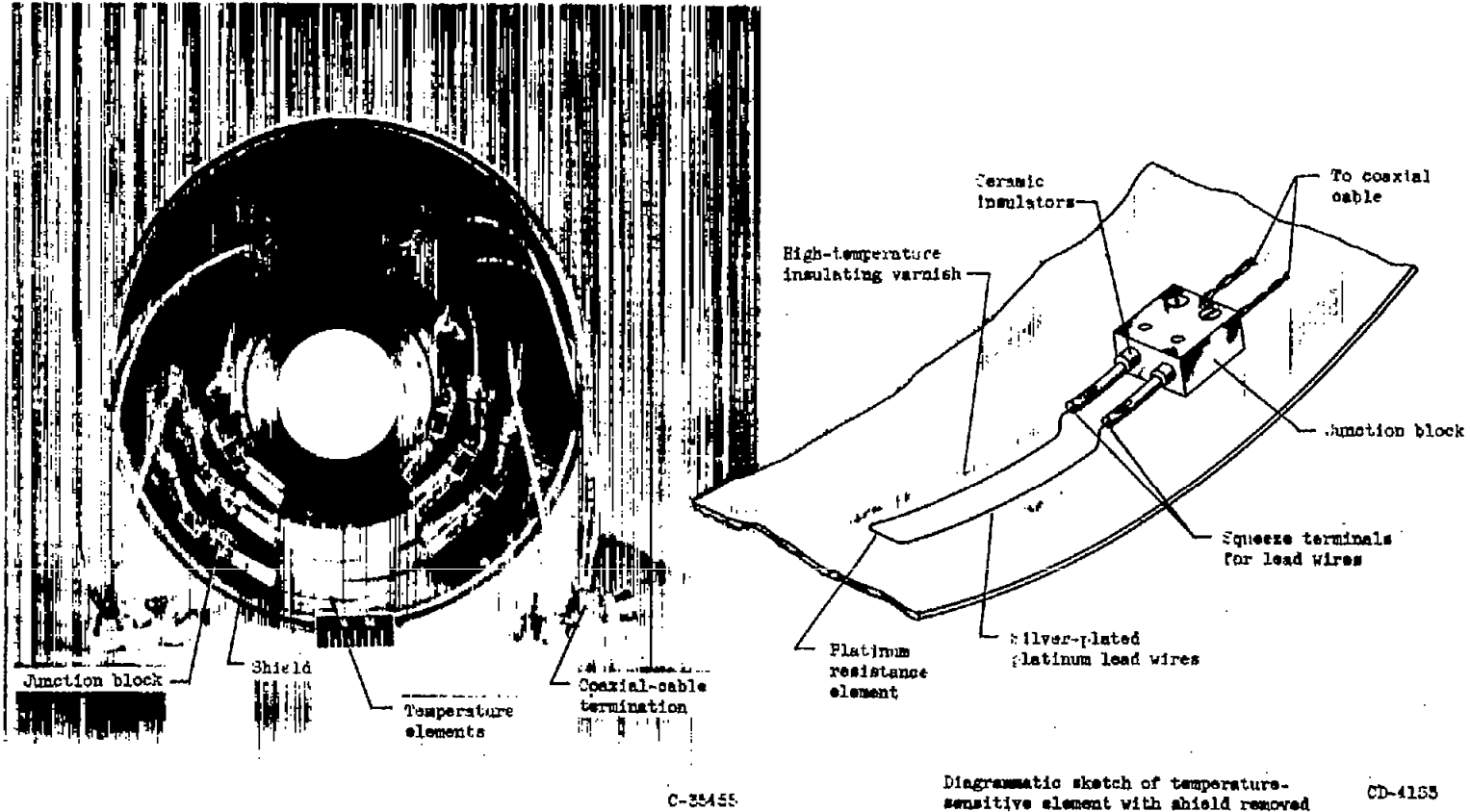


Figure 4. - Typical installation of resistance-wire temperature elements as installed in model 3.

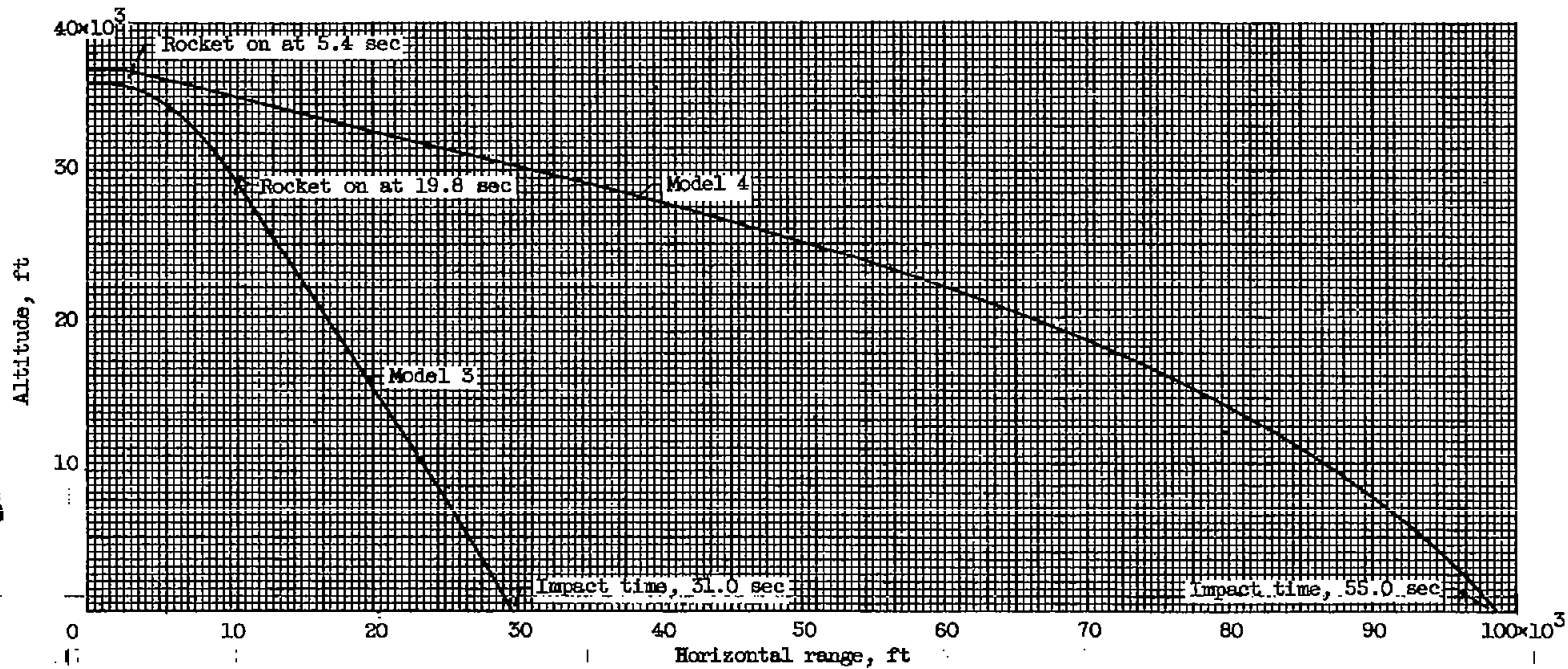
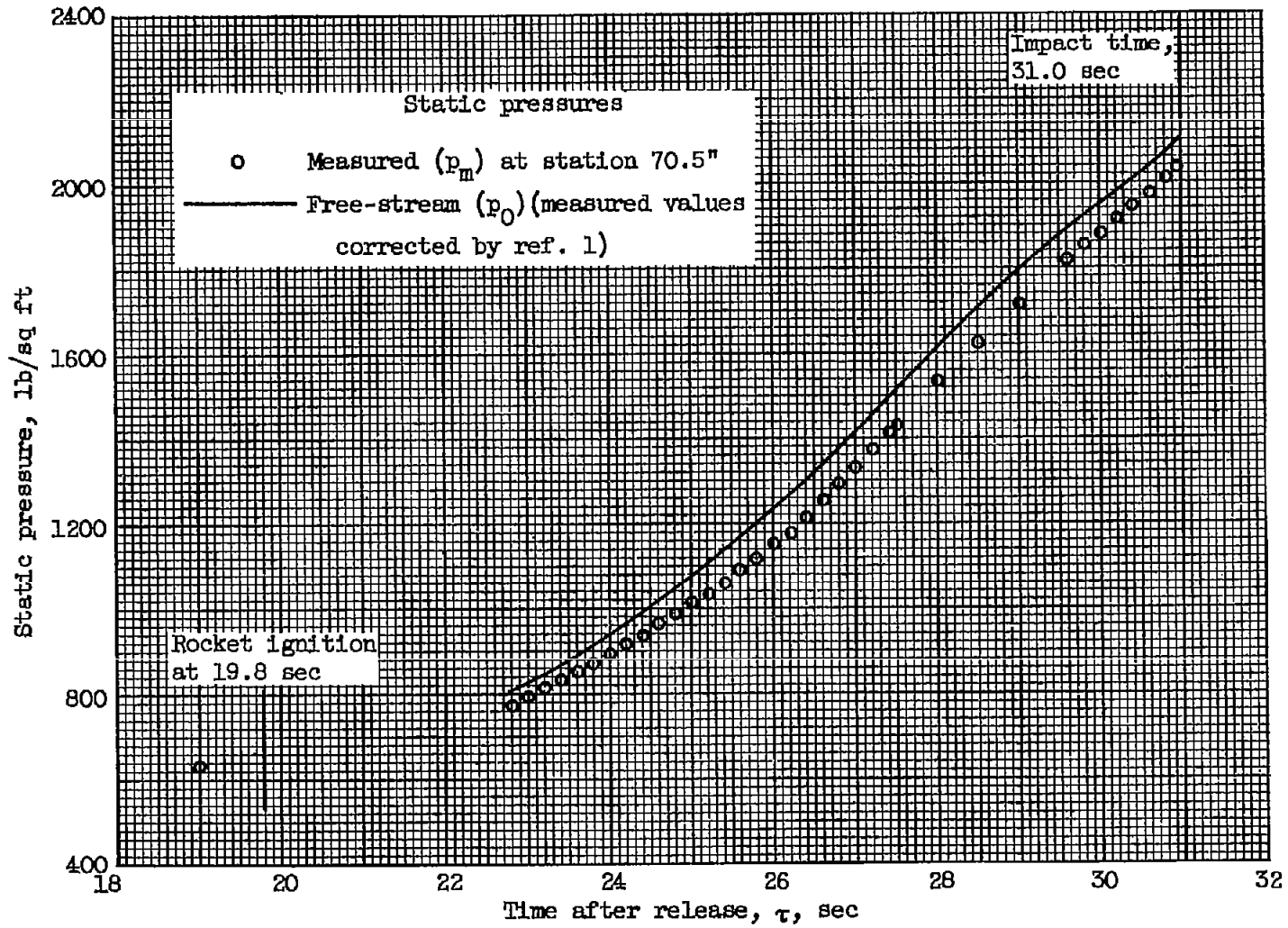
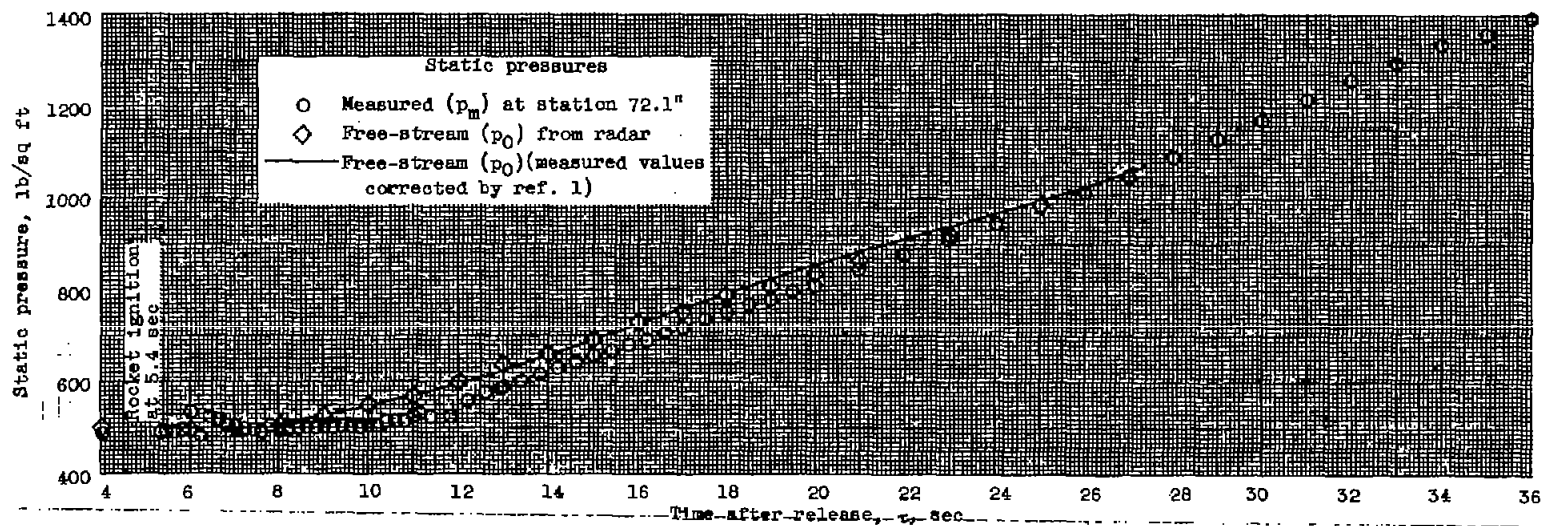


Figure 5. - Trajectories of models 3 and 4.



(a) Model 3.

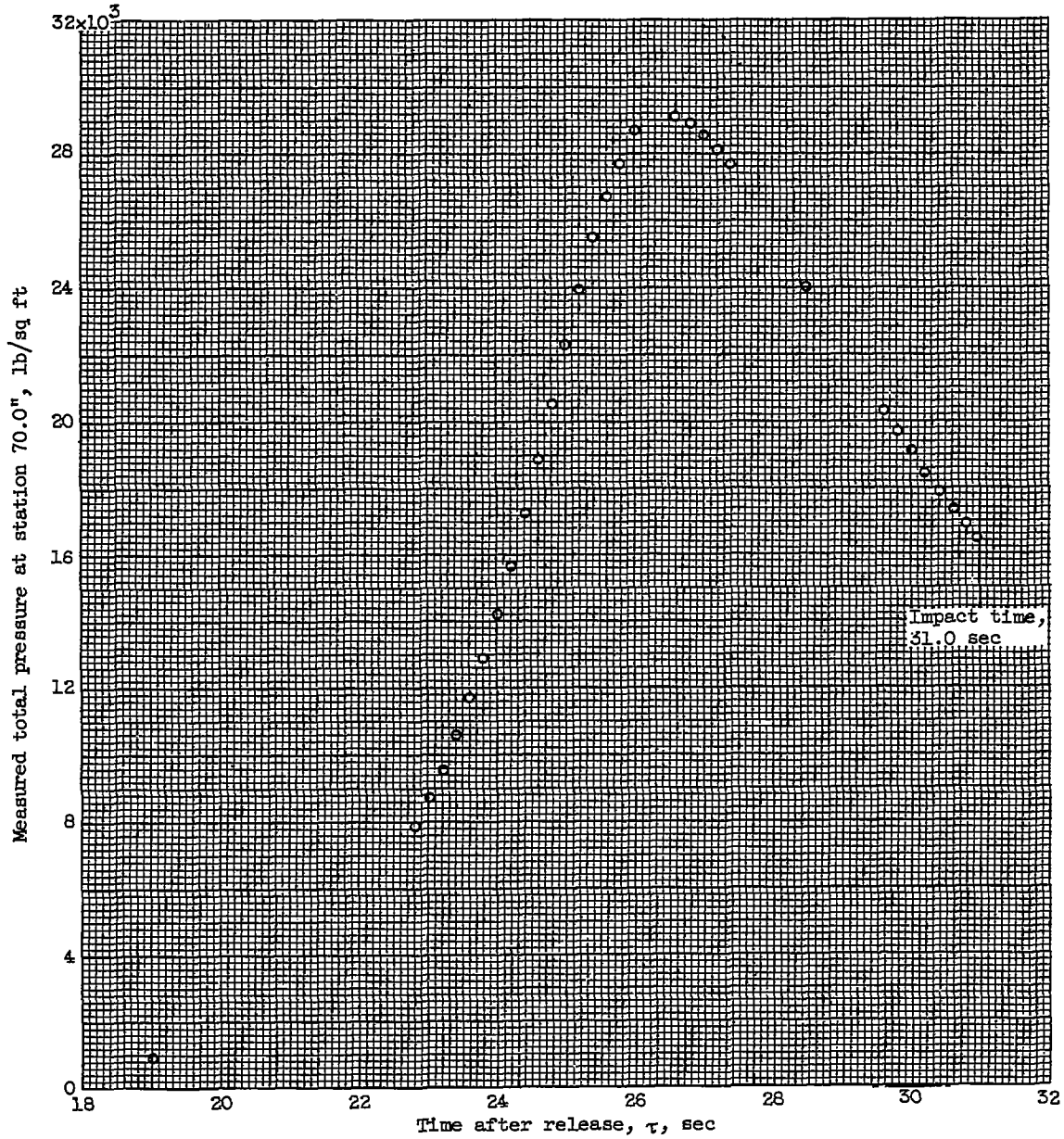
Figure 6. - Time history of free-stream static pressure.



(b) Model 4.

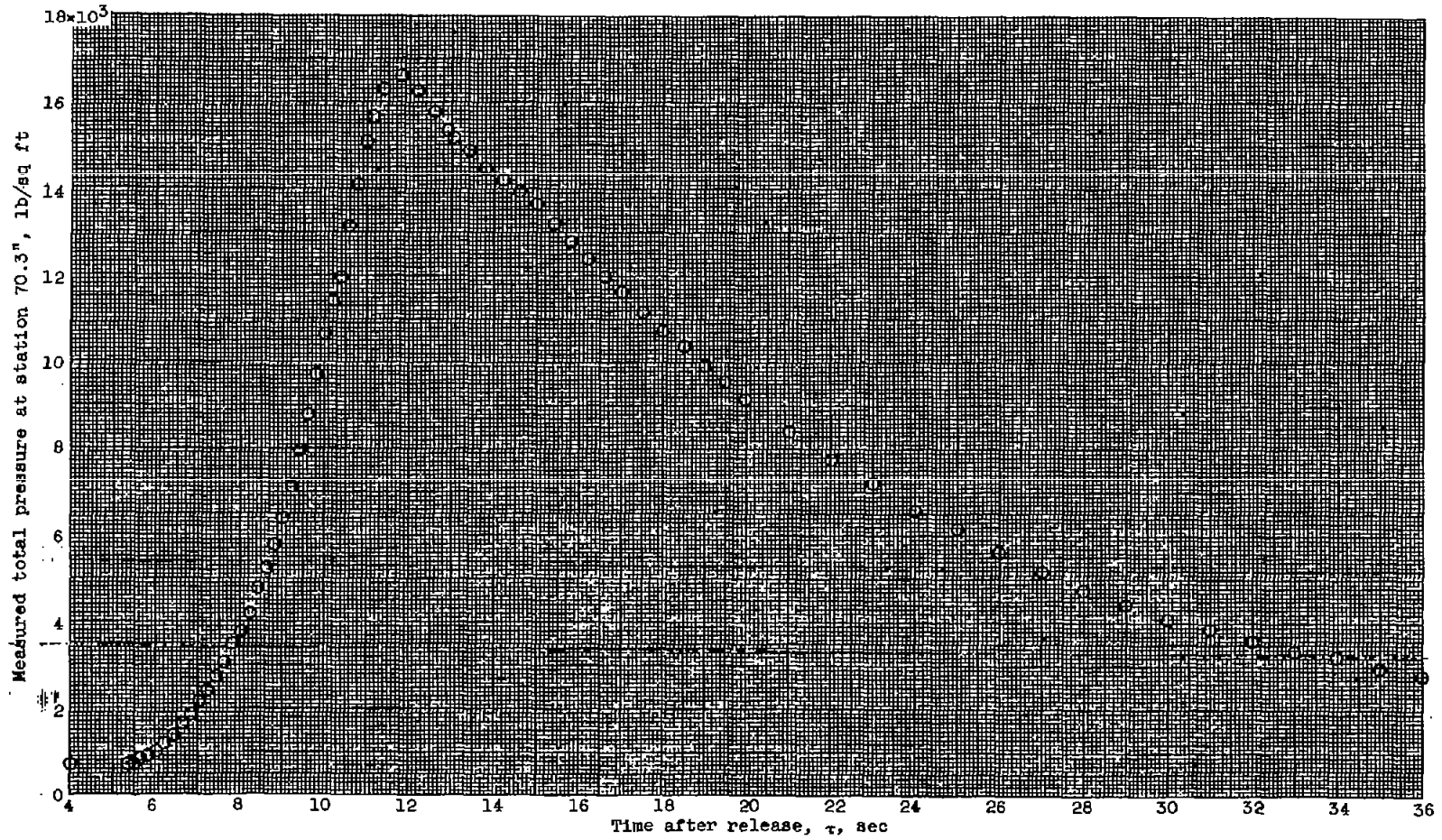
Figure 8. - Concluded. Time history of free-stream static pressure.

1961



(a) Model 3.

Figure 7. - Time history of measured total pressure.



(b) Model 4.

Figure 7. - Concluded. Time history of measured total pressure.

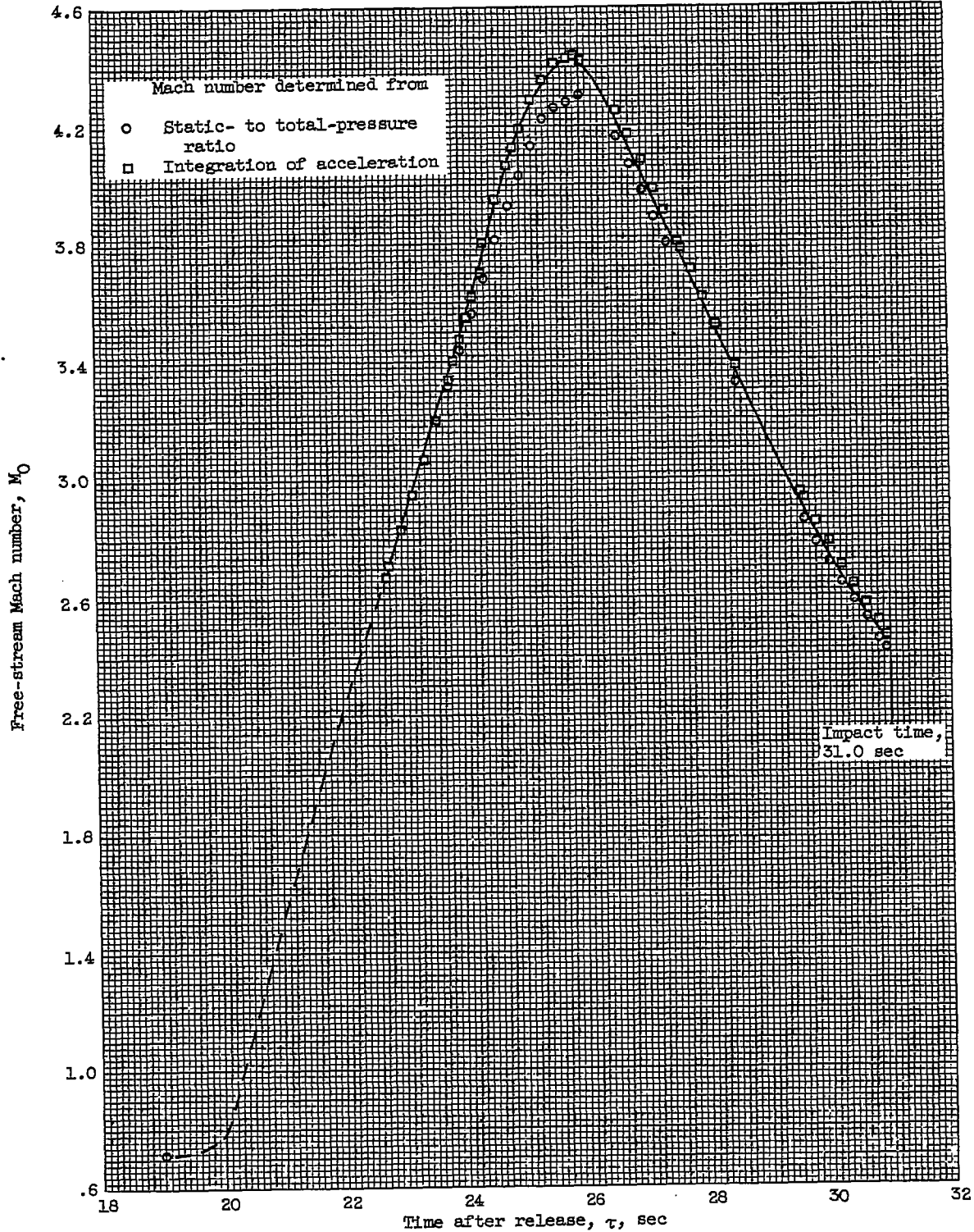
CONFIDENTIAL

CONFIDENTIAL

NACA RM E55P27

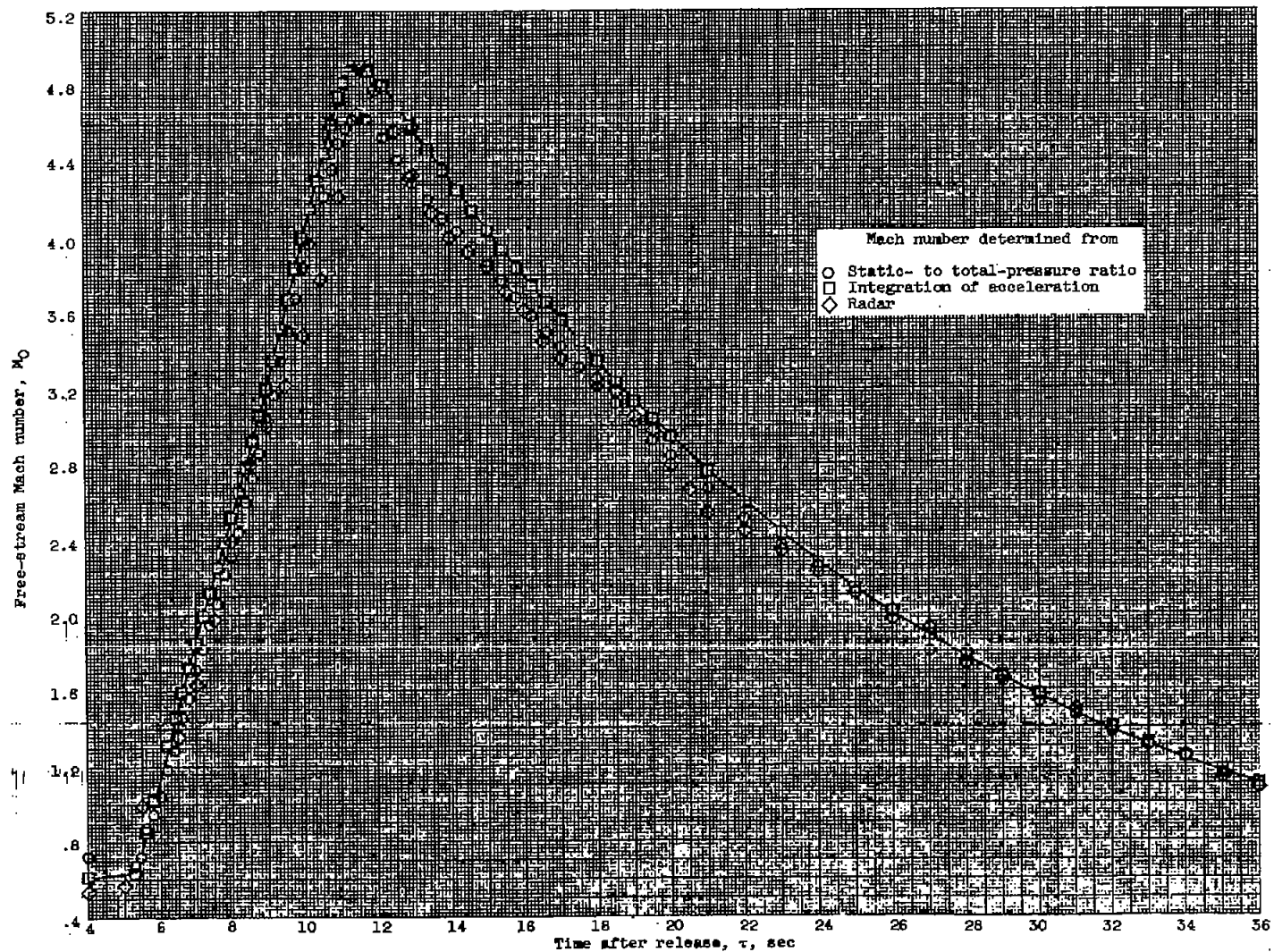
3661

CF-4



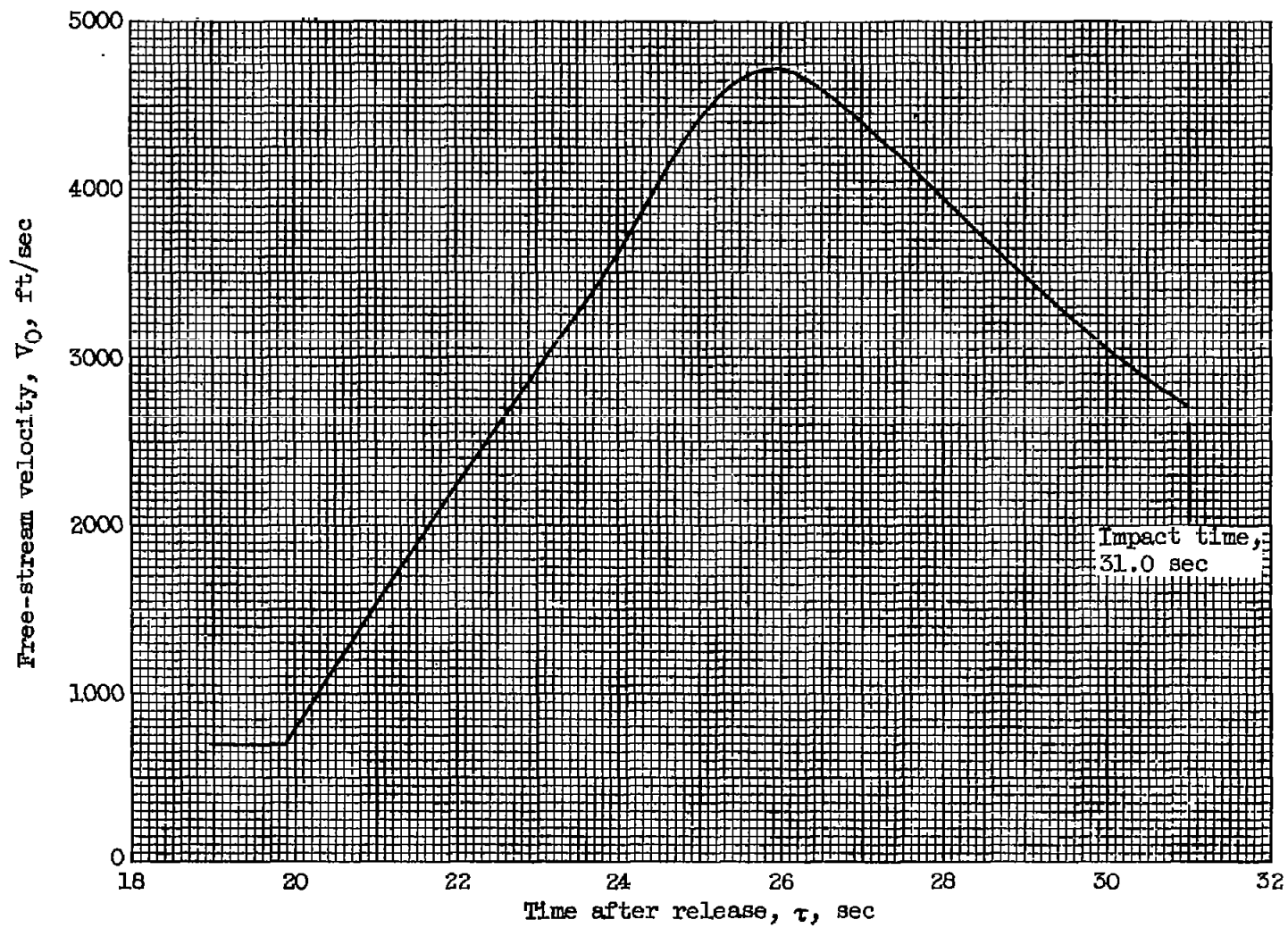
(a) Model 3.

Figure 8. - Time history of free-stream Mach number.



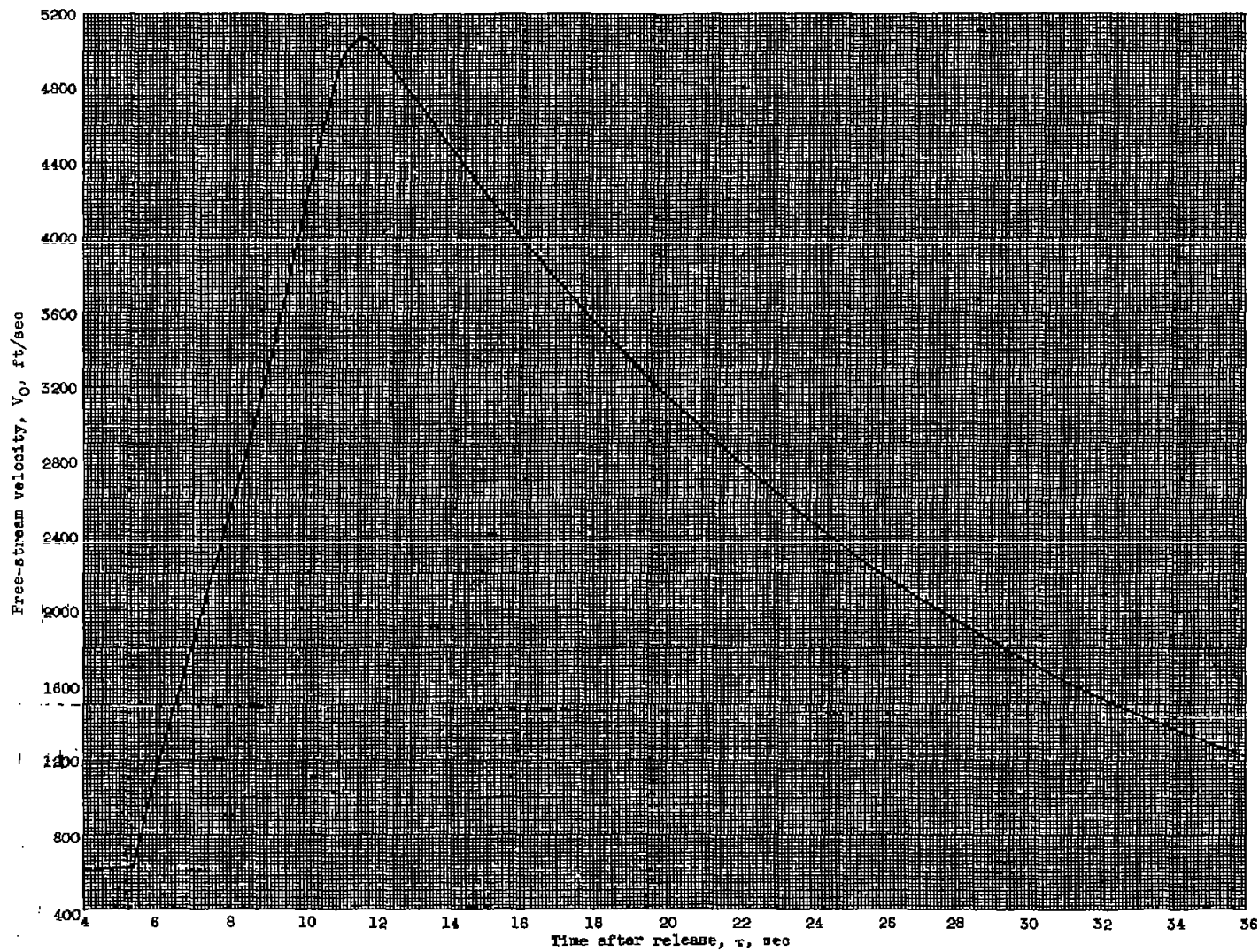
(b) Model 4.

Figure 8. - Concluded. Time history of free-stream Mach number.



(a) Model 3.

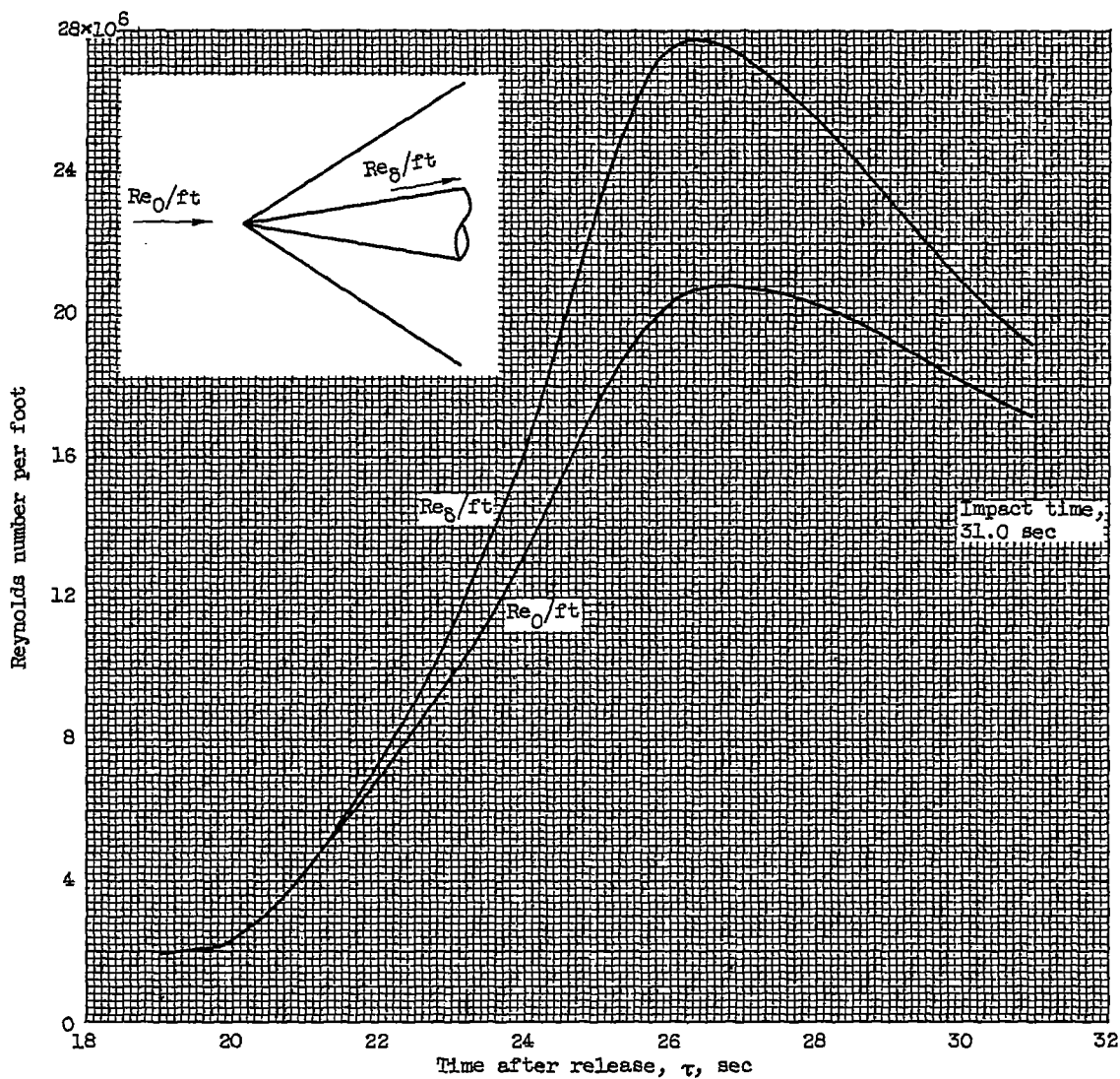
Figure 9. - Time history of free-stream velocity.



(b) Model 4.

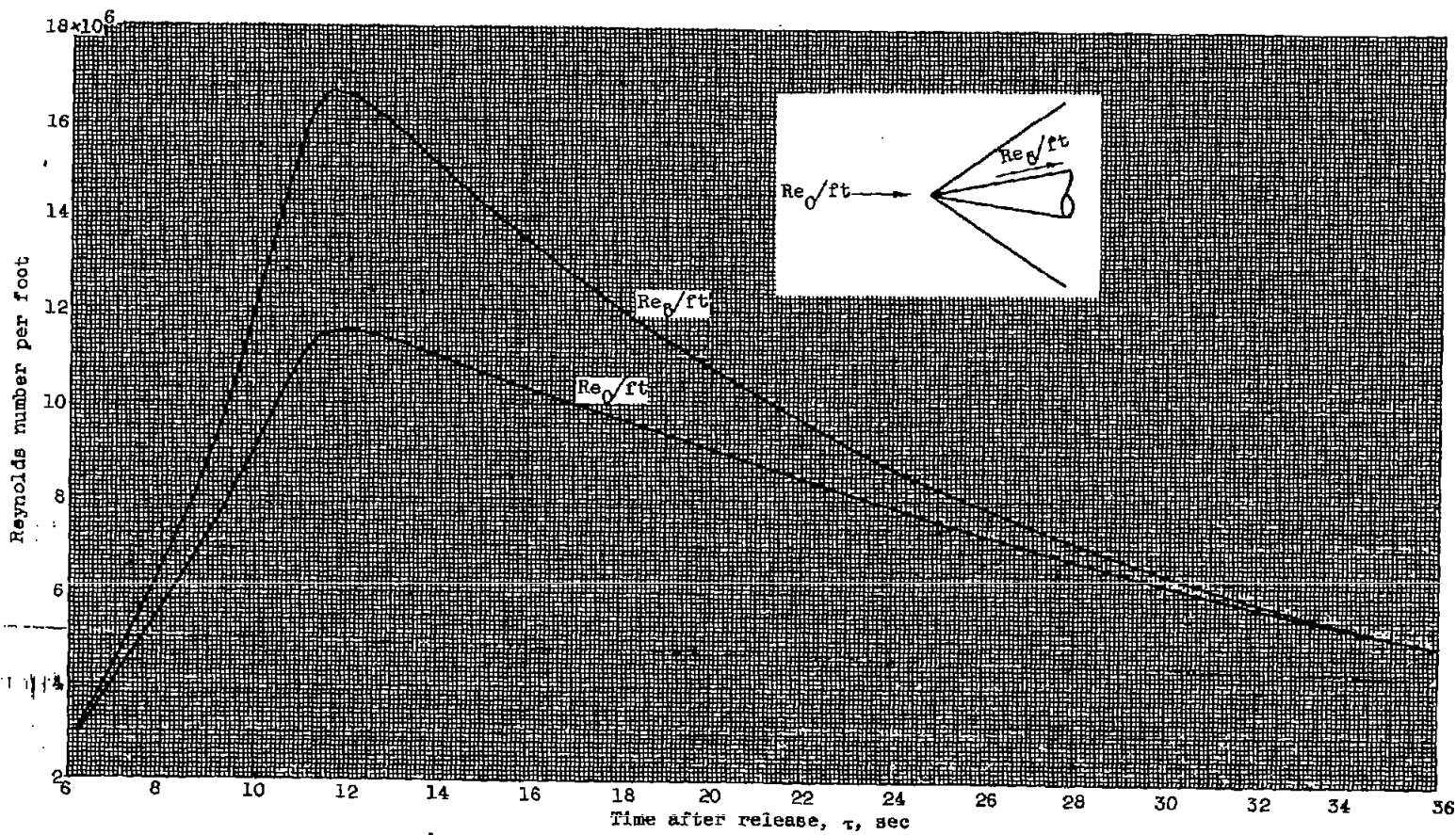
Figure 9. - Concluded. Time history of free-stream velocity.

3661



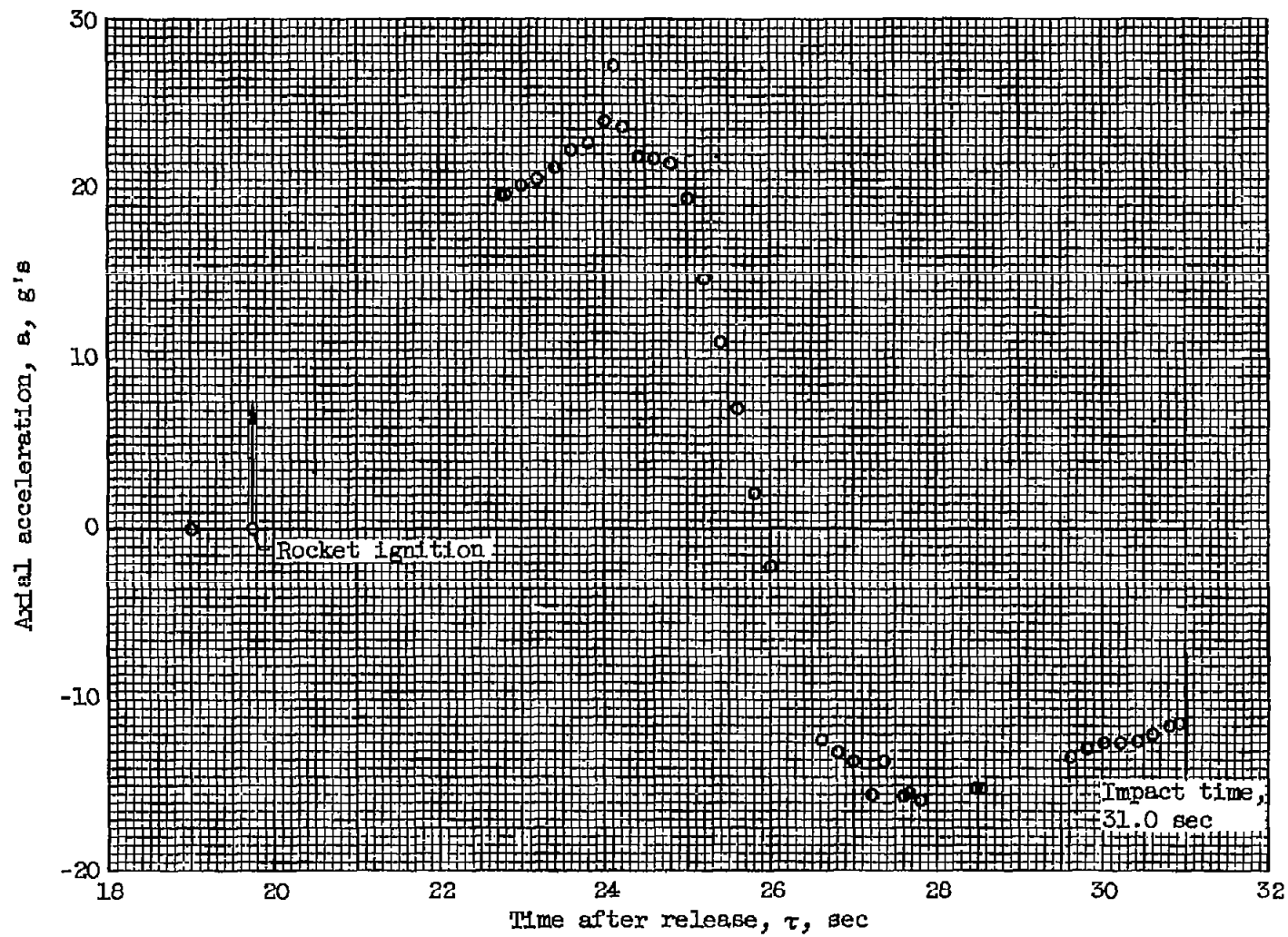
(a) Model 3.

Figure 10. - Time history of free-stream Reynolds number per foot and cone Reynolds number per foot.



(b) Model 4.

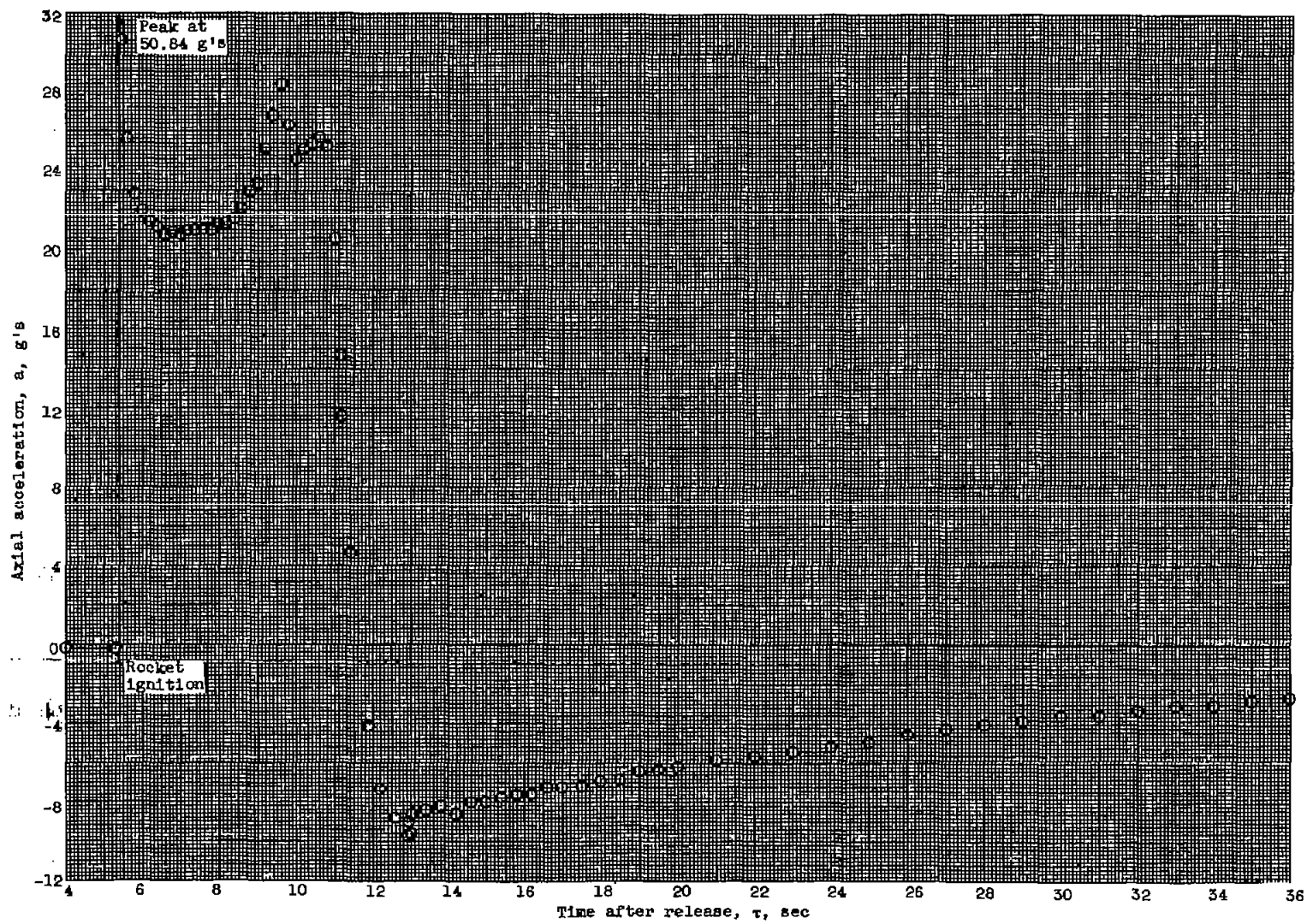
Figure 10. - Concluded. Time history of free-stream Reynolds number per foot and cone Reynolds number per foot.



(a) Model 3.

Figure 11. - Time history of axial acceleration.

CONFIDENTIAL



(b) Model 4.

Figure 11. - Concluded. Time history of axial acceleration.

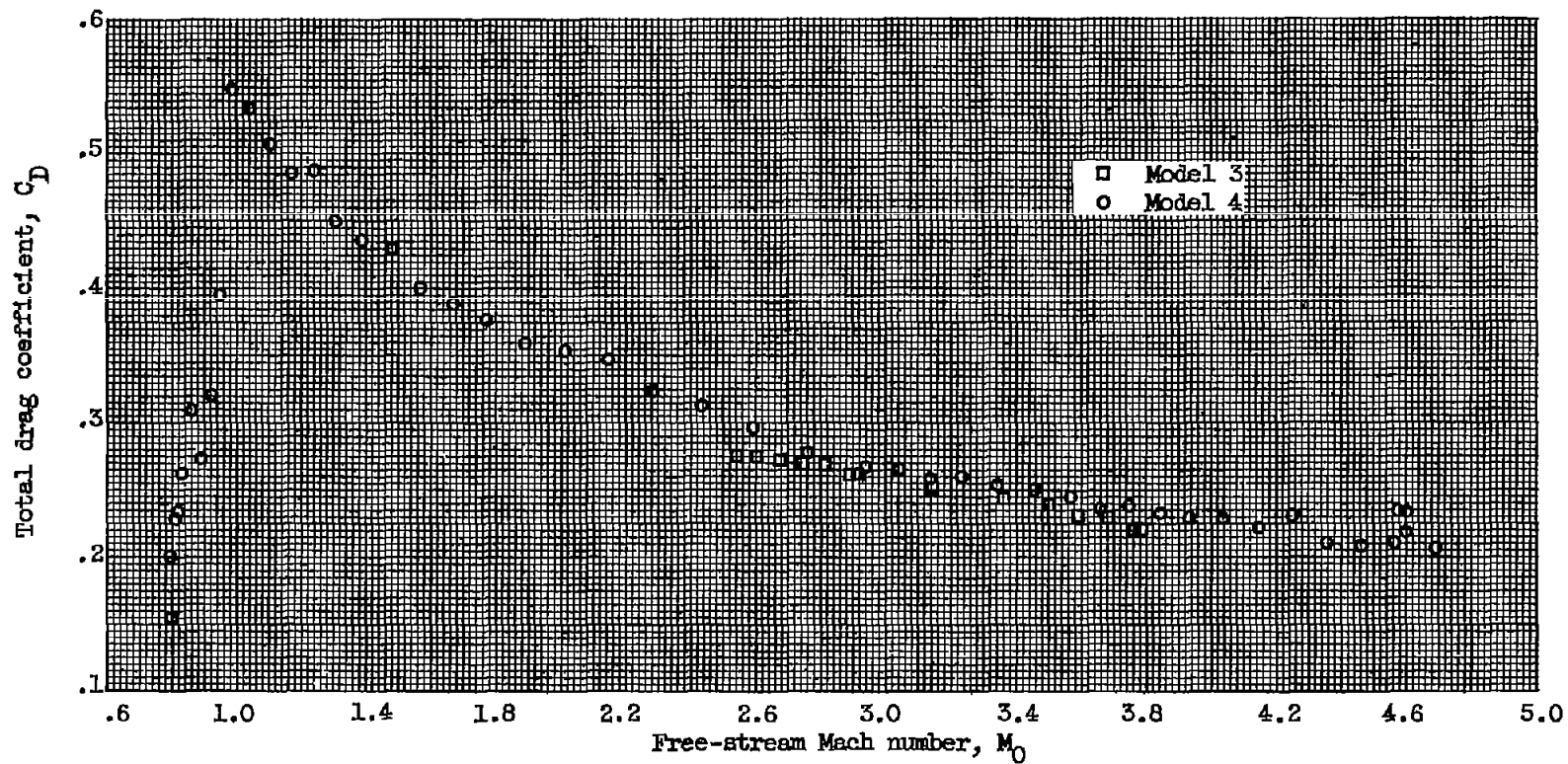
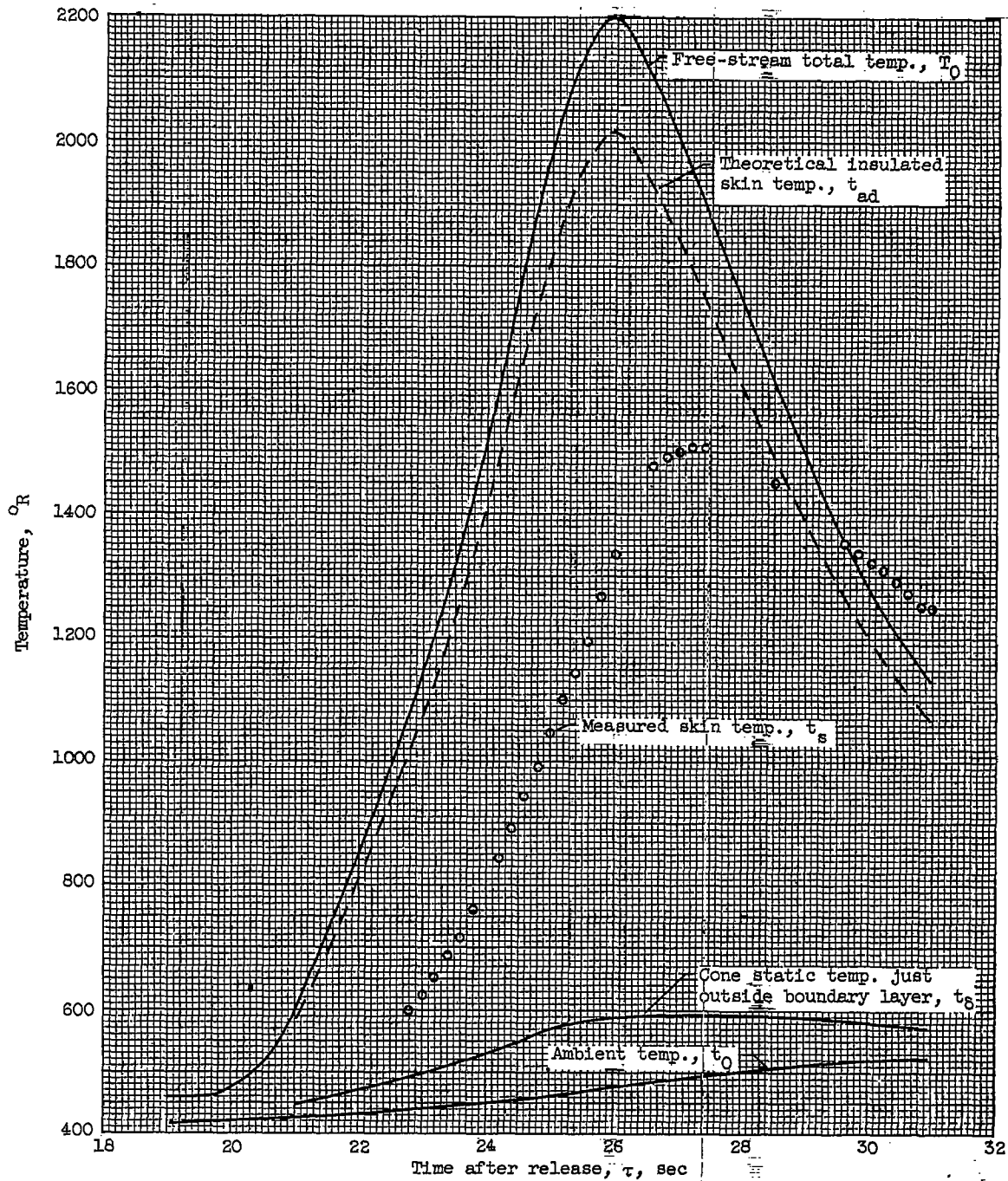


Figure 12. - Total drag coefficient against free-stream Mach number during deceleration portion of flight.

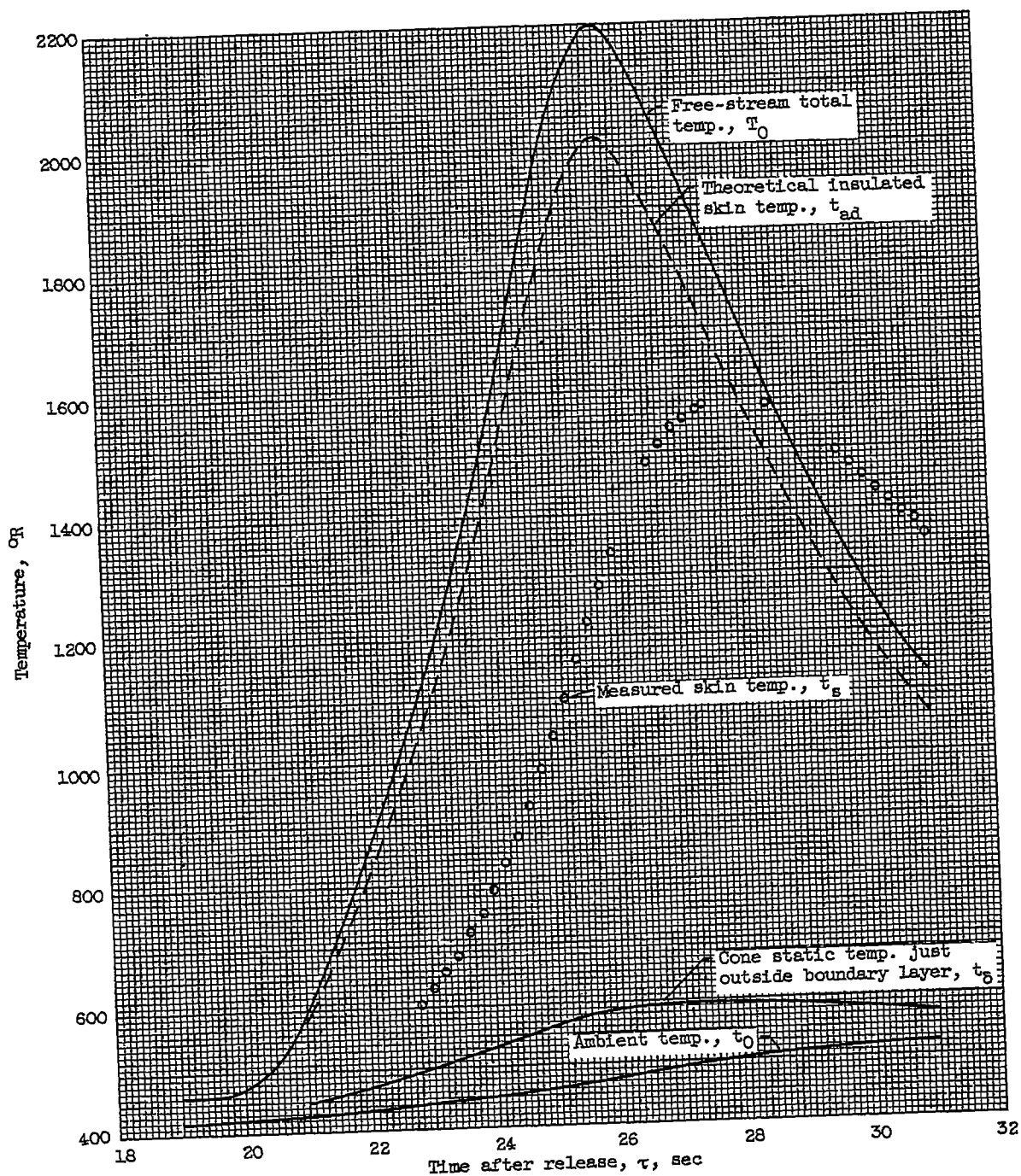


(a) Slant distance from cone apex, 14.46 inches.

Figure 13. - Time history of air and skin temperatures for model 3.

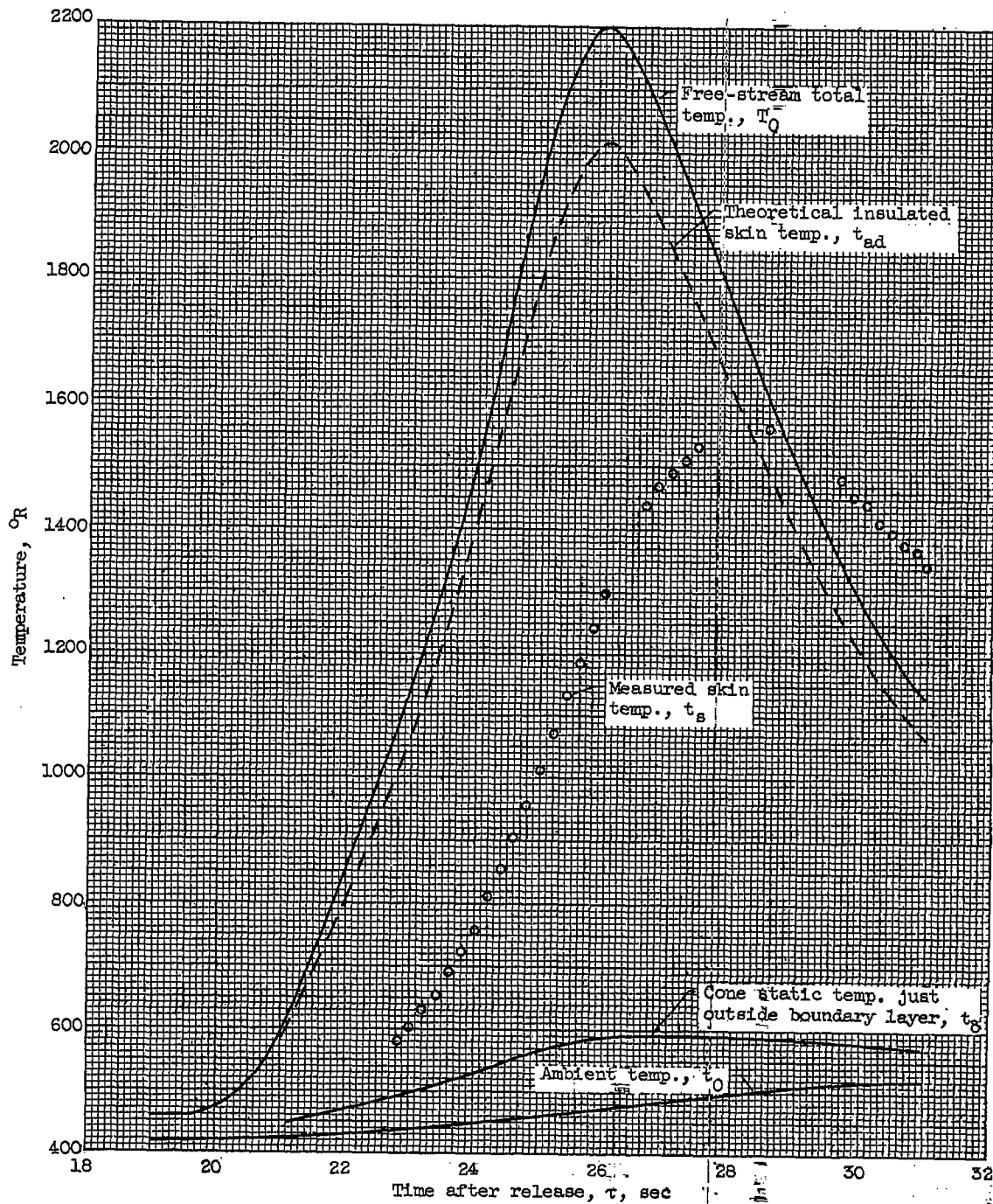
3661

CF-5 back



(b) Slant distance from cone apex, 18.40 inches.

Figure 13. - Continued. Time history of air and skin temperatures for model 3.

~~CONFIDENTIAL~~

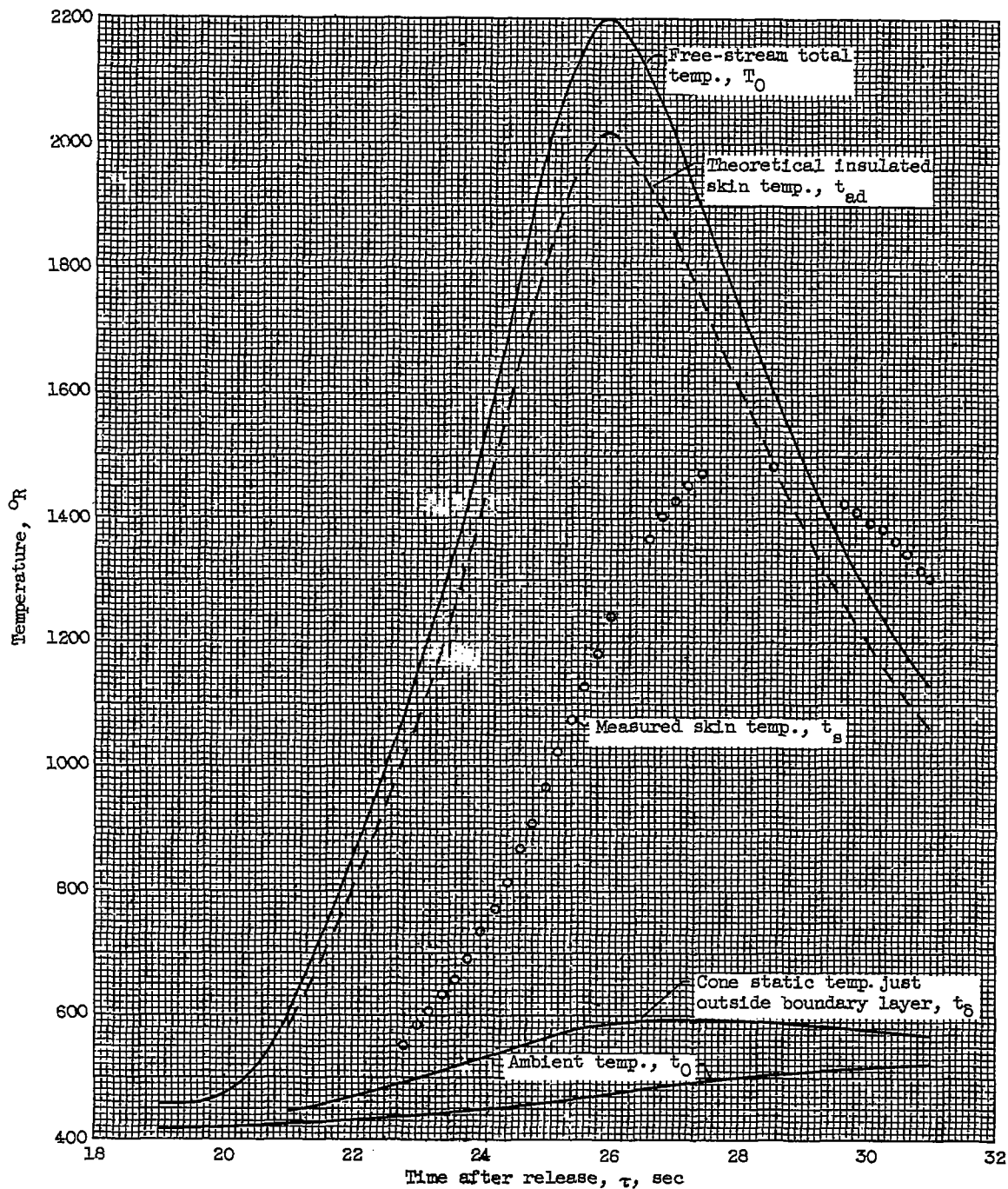
(c) Slant distance from cone apex, 20.34 inches.

Figure 13. - Continued. Time history of air and skin temperatures for model 3.

~~CONFIDENTIAL~~

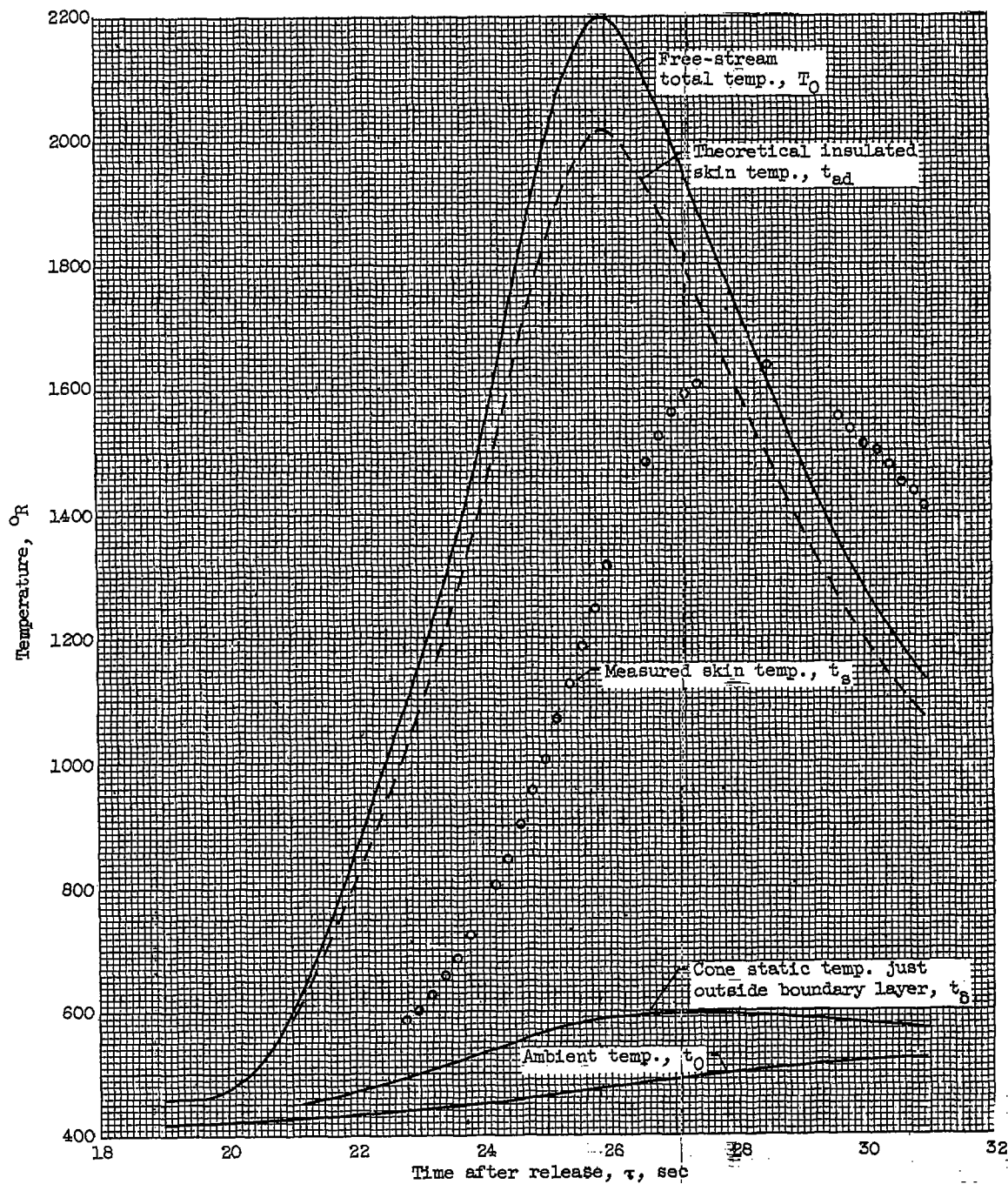
3661

3661  
T999C



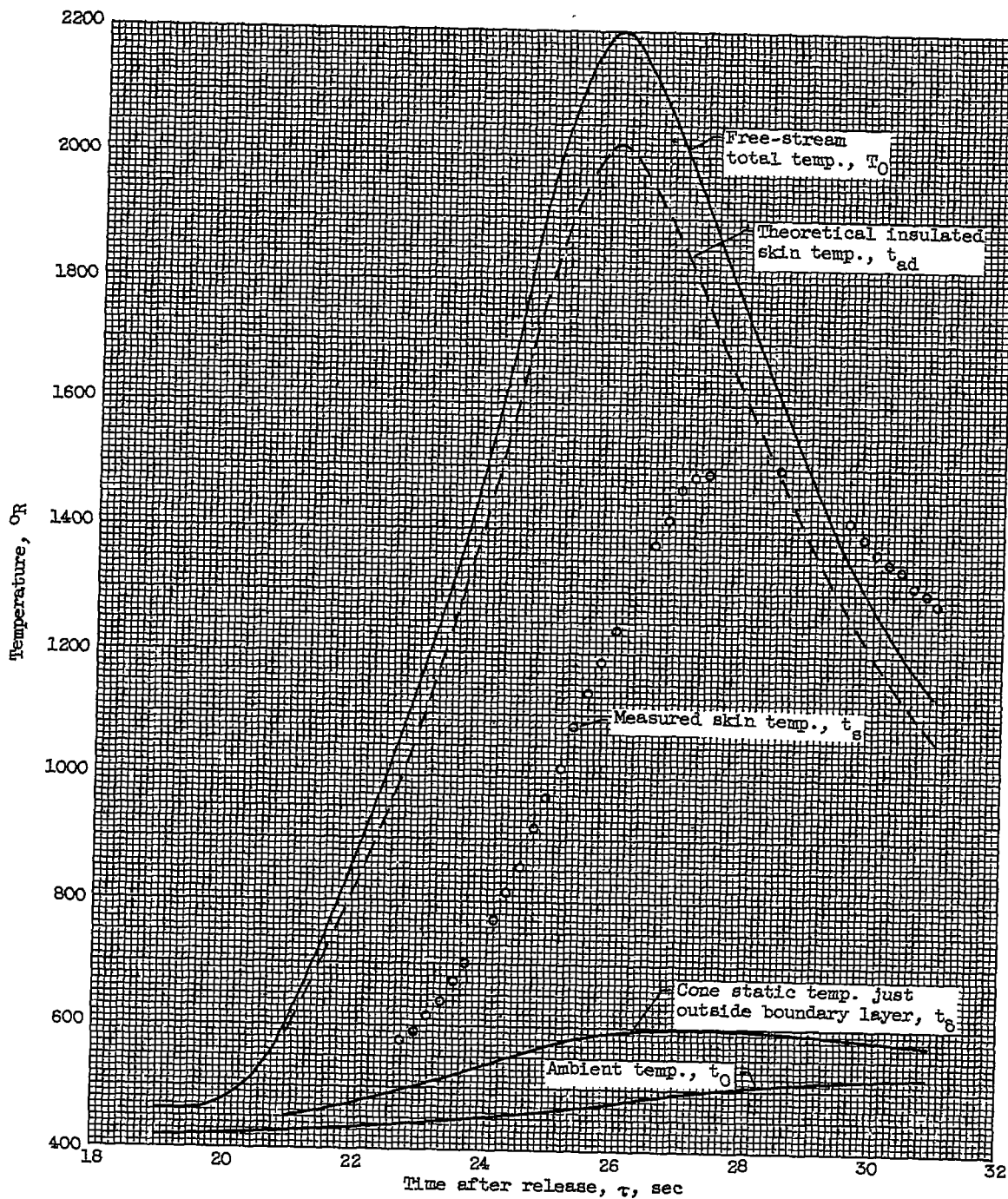
(d) Slant distance from cone apex, 22.34 inches.

Figure 13. - Continued. Time history of air and skin temperatures for model 3.



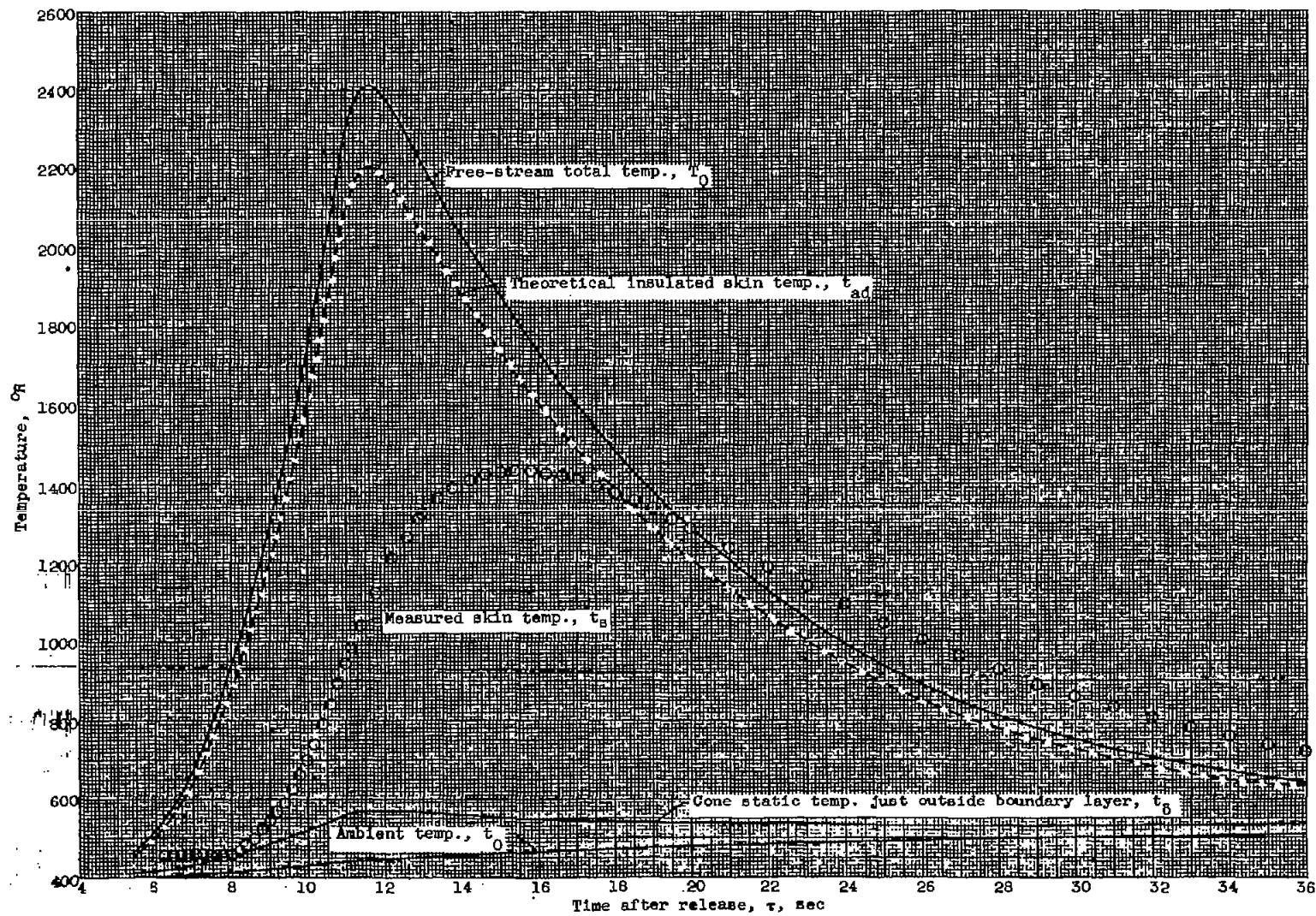
(e) Slant distance from cone apex, 24.21 inches.

Figure 13. - Continued. Time history of air and skin temperatures for model 3.



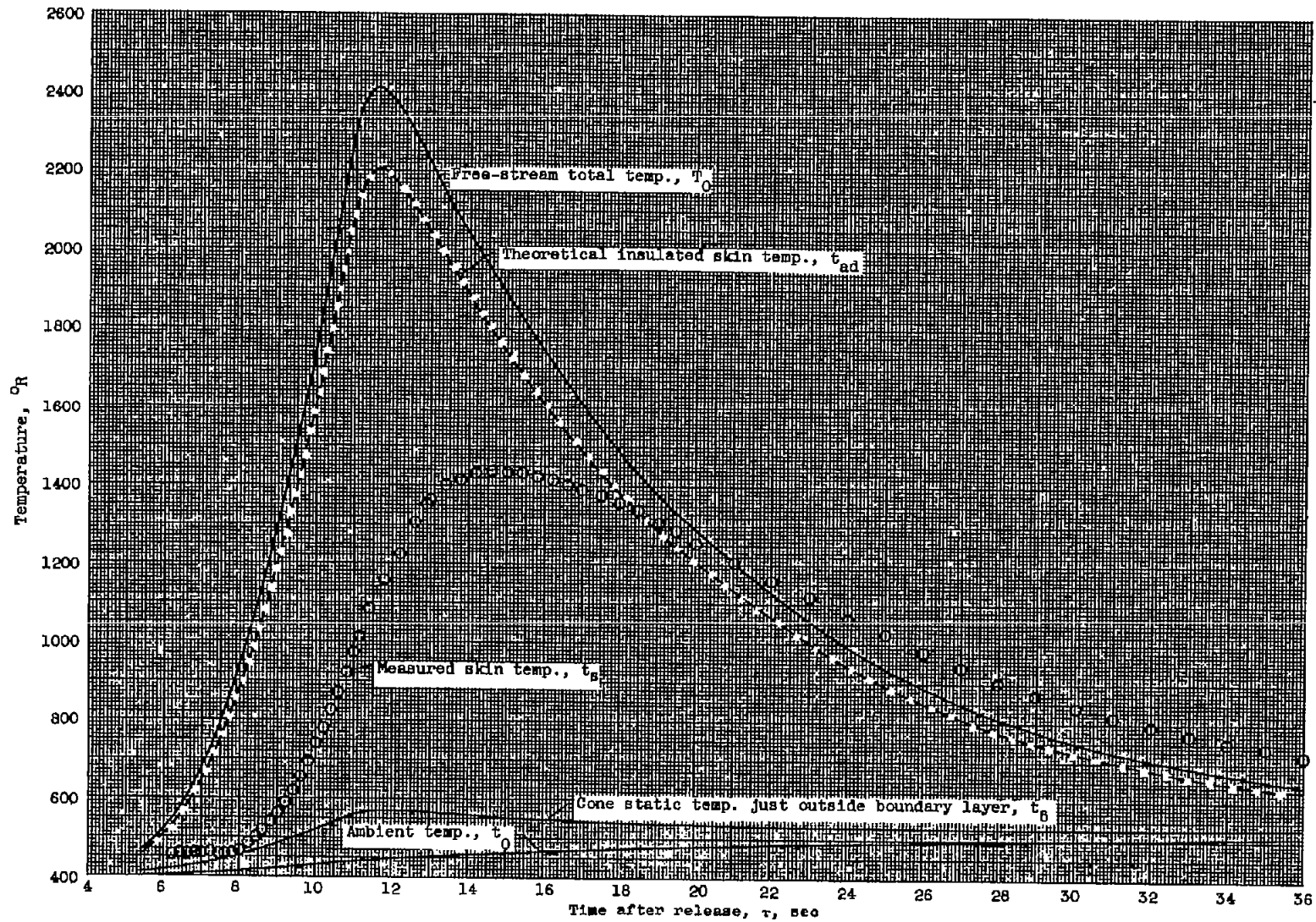
(f) Slant distance from cone apex, 25.96 inches.

Figure 13. - Concluded. Time history of air and skin temperatures for model 3.



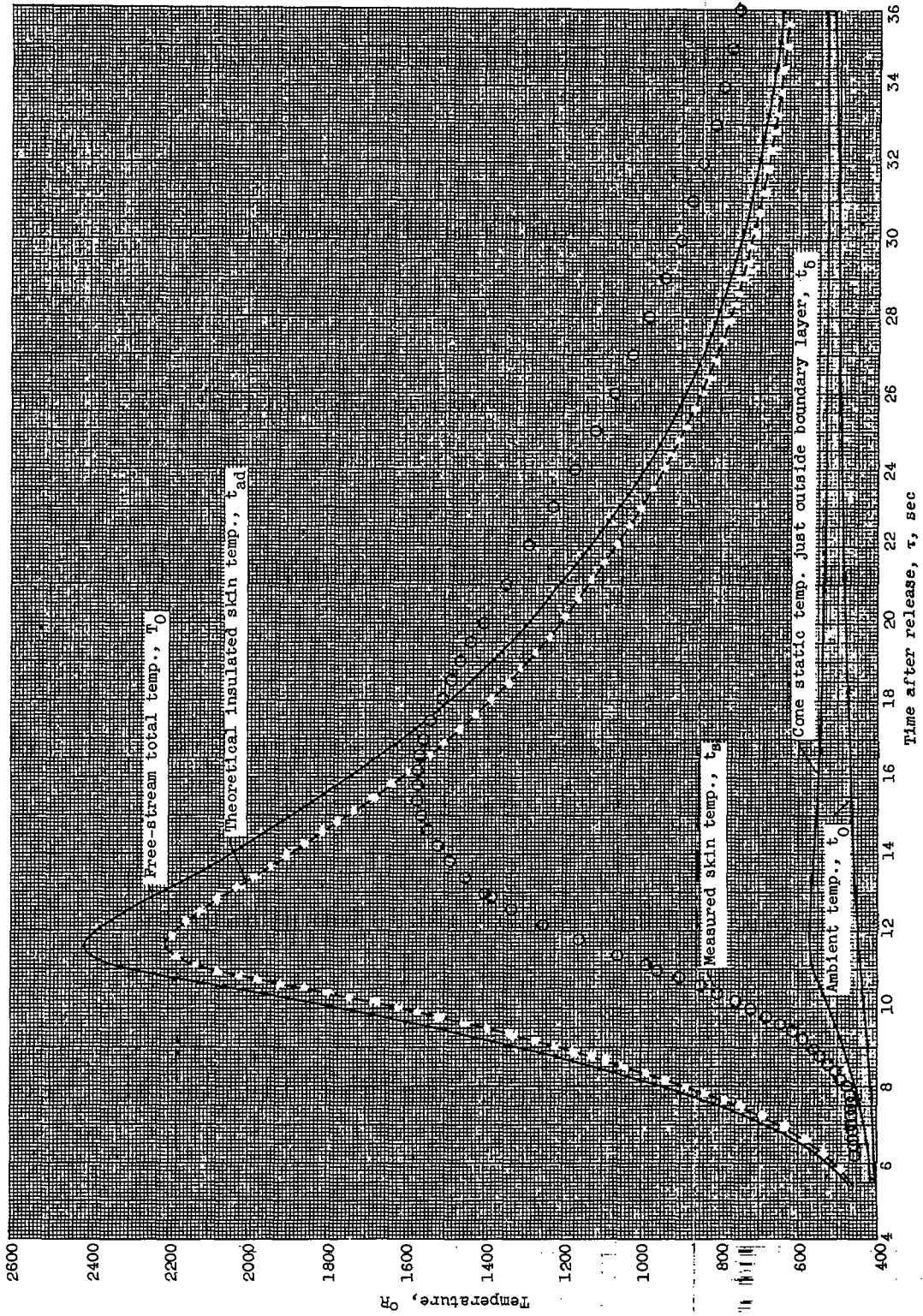
(a) Slant distance from cone apex, 15.29 inches.

Figure 14. - Time history of air and skin temperatures for model 4.



(b) Slant distance from cone apex, 16.23 inches.

Figure 14. - Continued. Time history of air and skin temperatures for model 4.

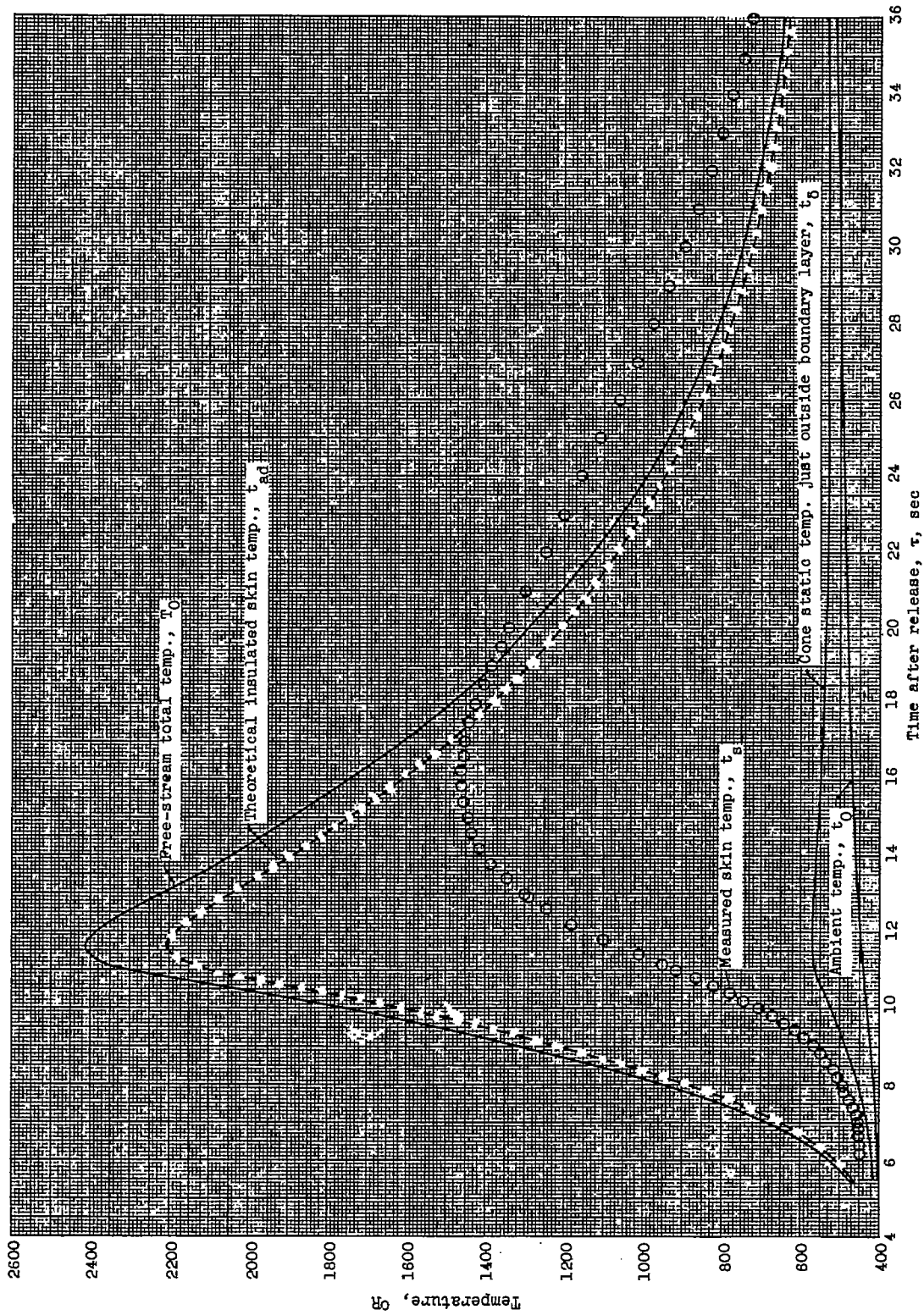


(c) Slant distance from cone apex, 17.23 inches.

Figure 14. - Continued. Time history of air and skin temperatures for model 4.

3661

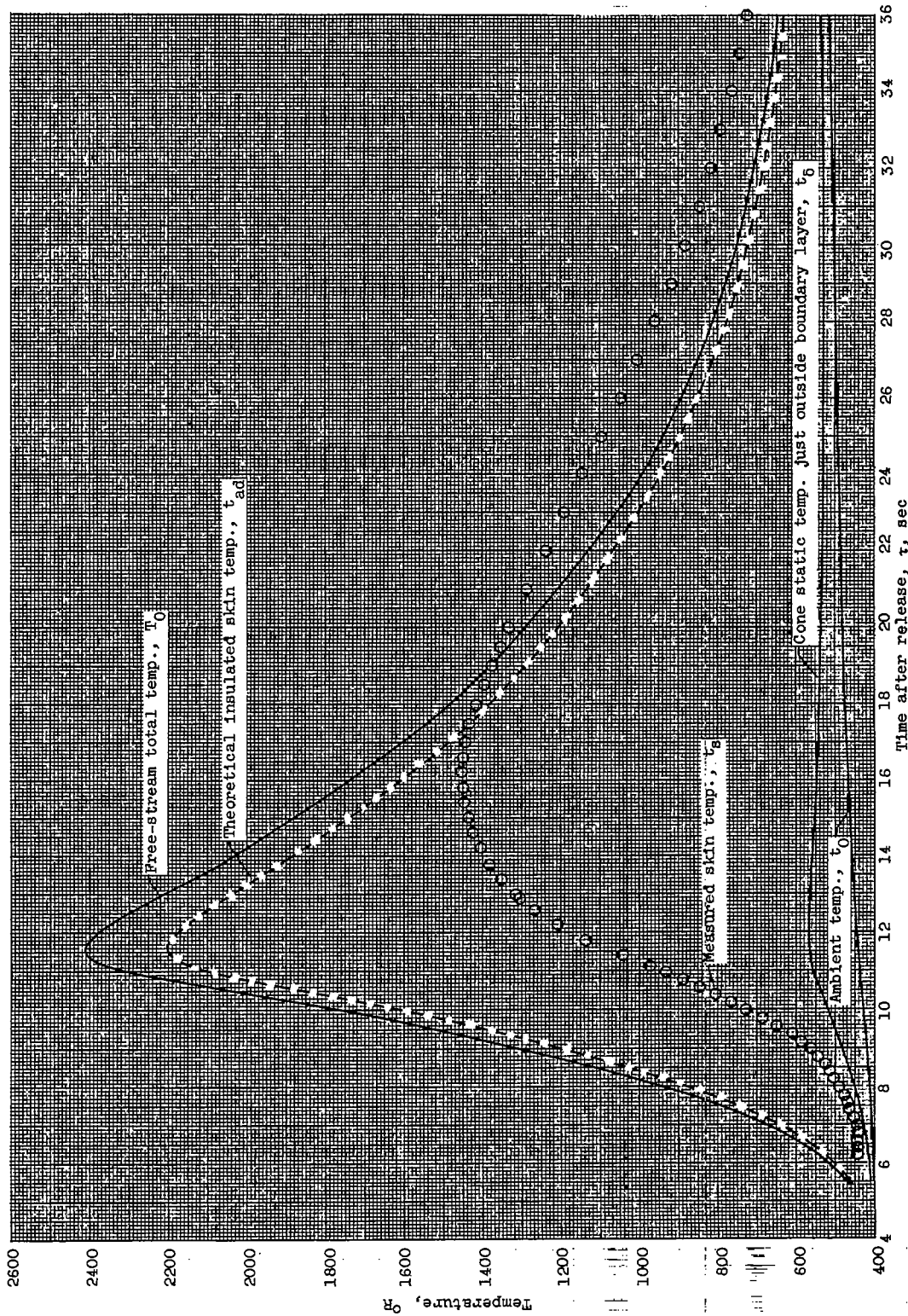
EF-6 back



(d) Slant distance from cone apex, 21.10 inches.

Figure 14. - Continued. Time history of air and skin temperatures for model 4.

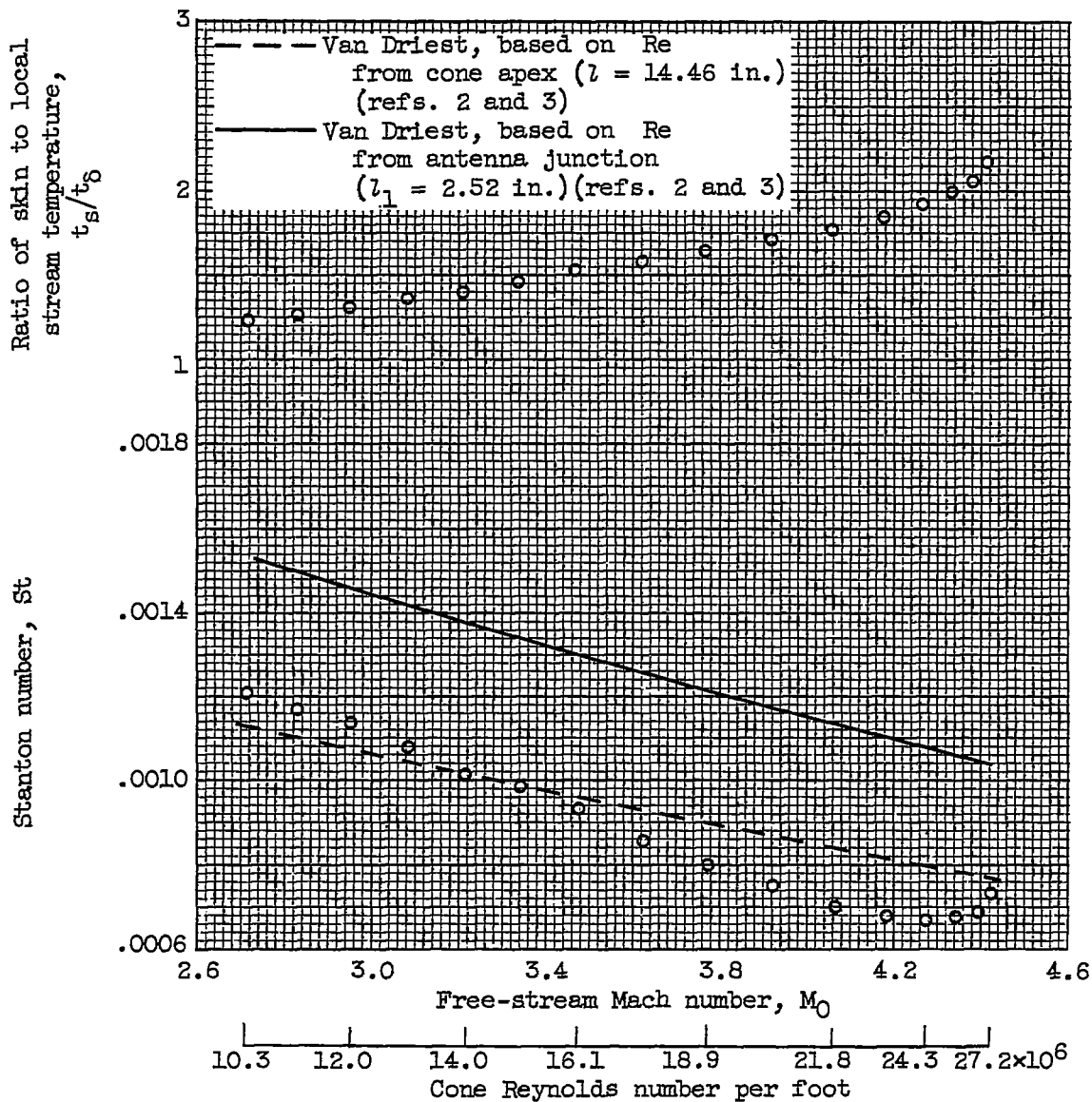
~~CONFIDENTIAL~~



(e) Slant distance from cone apex, 22.91 inches.

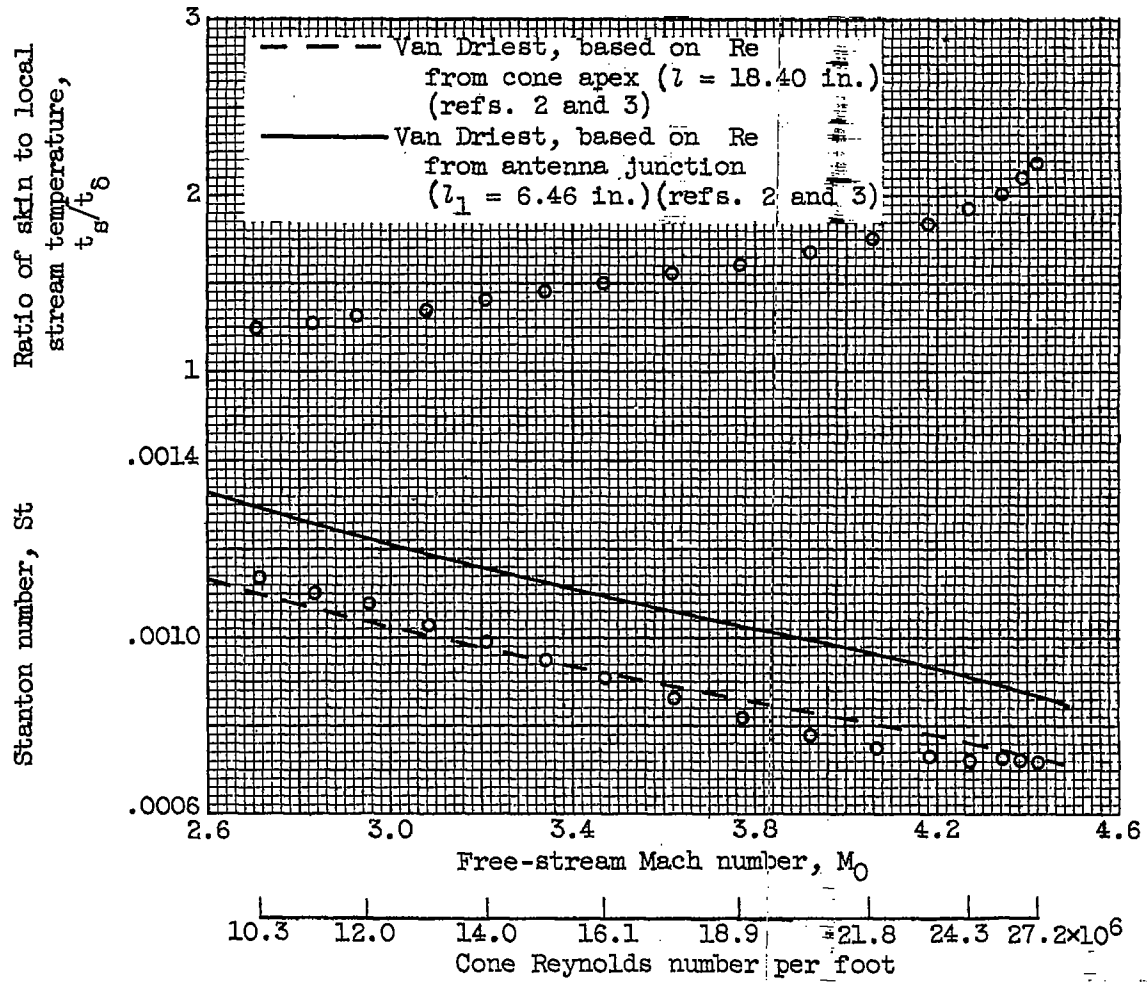
Figure 14. - Concluded. Time history of air and skin temperatures for model 4.

3661



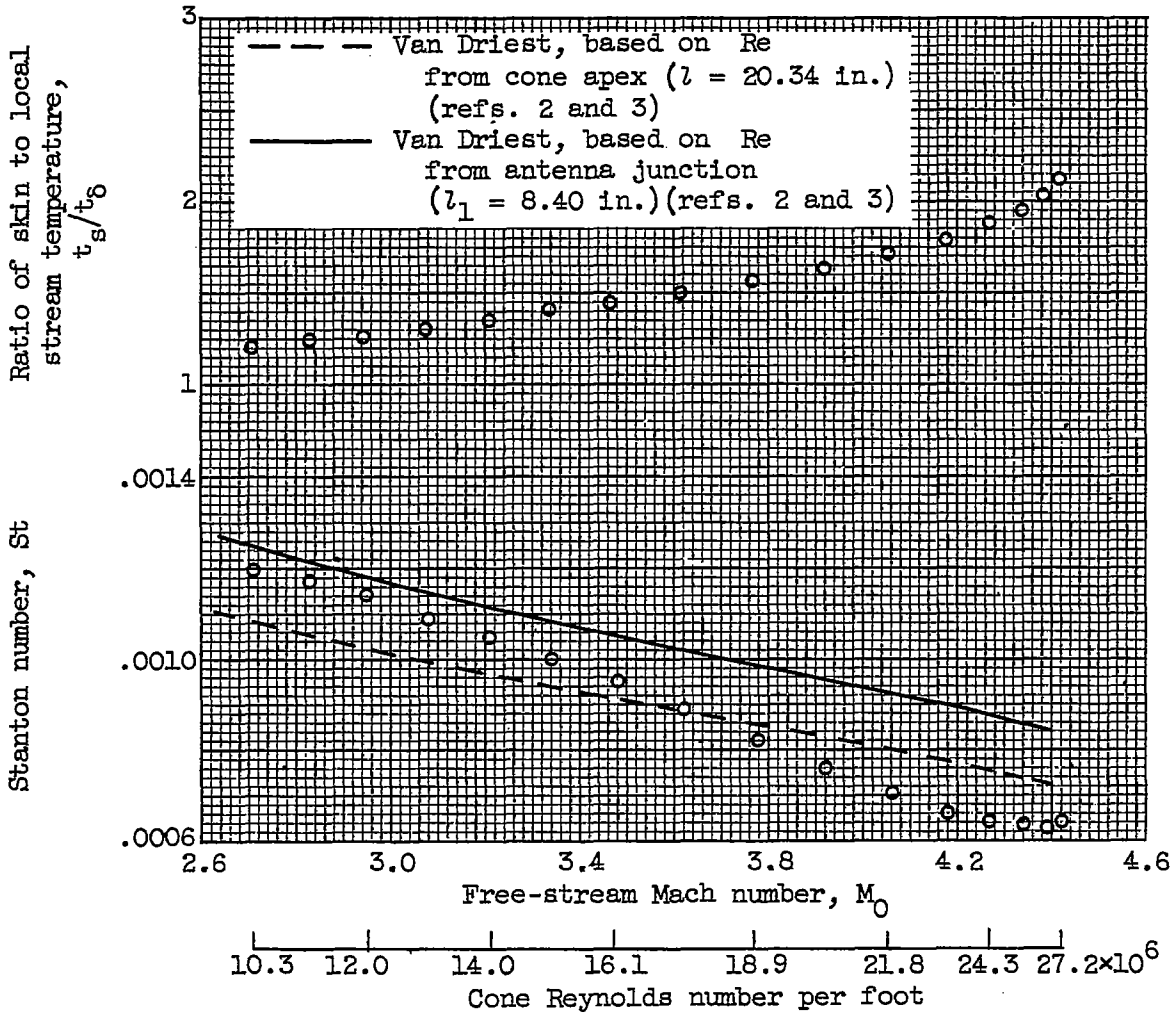
(a) Slant distance from cone apex, 14.46 inches.

Figure 15. - Ratio of skin to local stream temperature and Stanton number against free-stream Mach number and cone Reynolds number per foot for model 3..



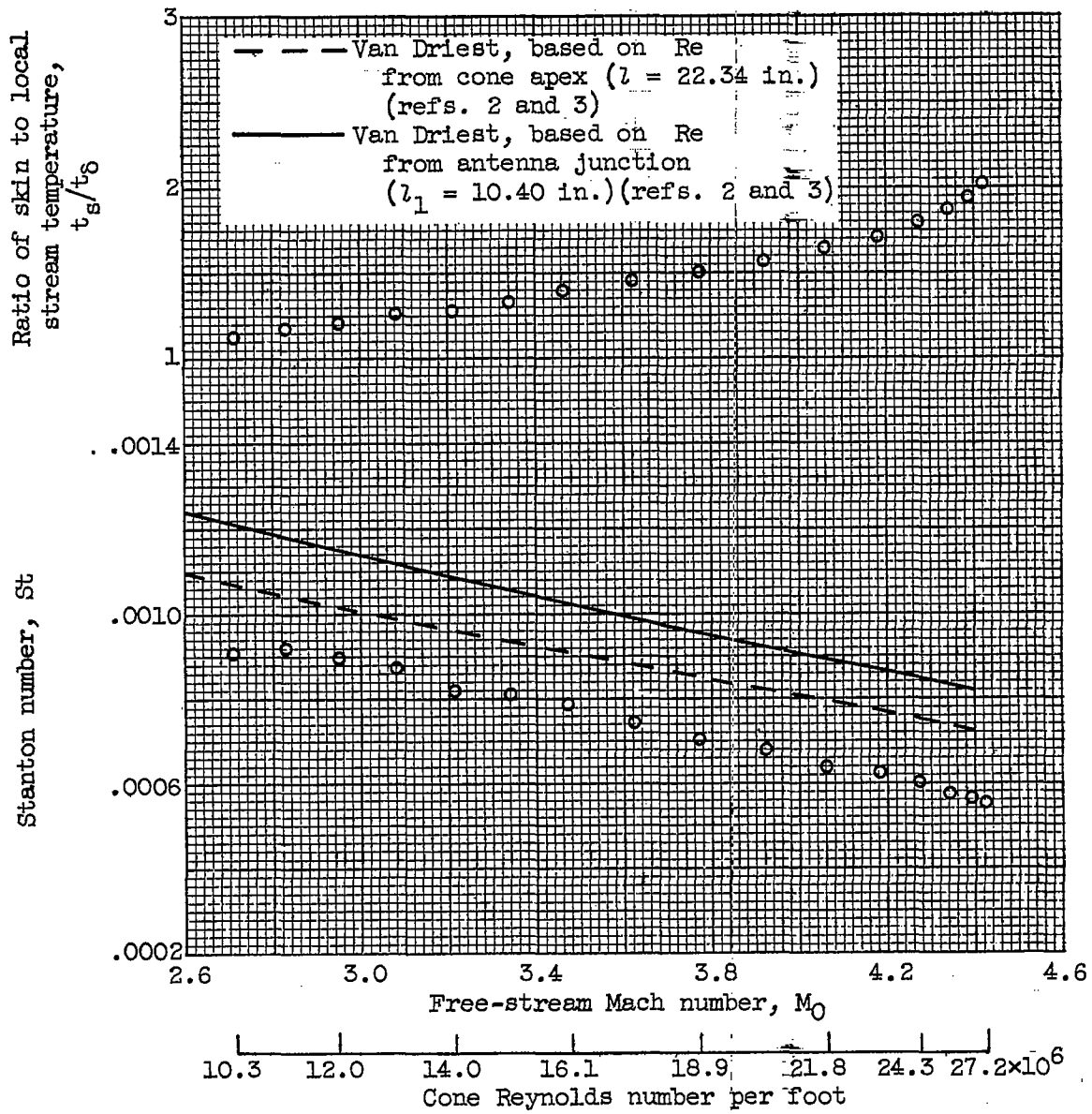
(b) Slant distance from cone apex, 18.40 inches.

Figure 15. - Continued. Ratio of skin to local stream temperature and Stanton number against free-stream Mach number and cone Reynolds number per foot for model 3.



(c) Slant distance from cone apex, 20.34 inches.

Figure 15. - Continued. Ratio of skin to local stream temperature and Stanton number against free-stream Mach number and cone Reynolds number per foot for model 3.

~~CONFIDENTIAL~~

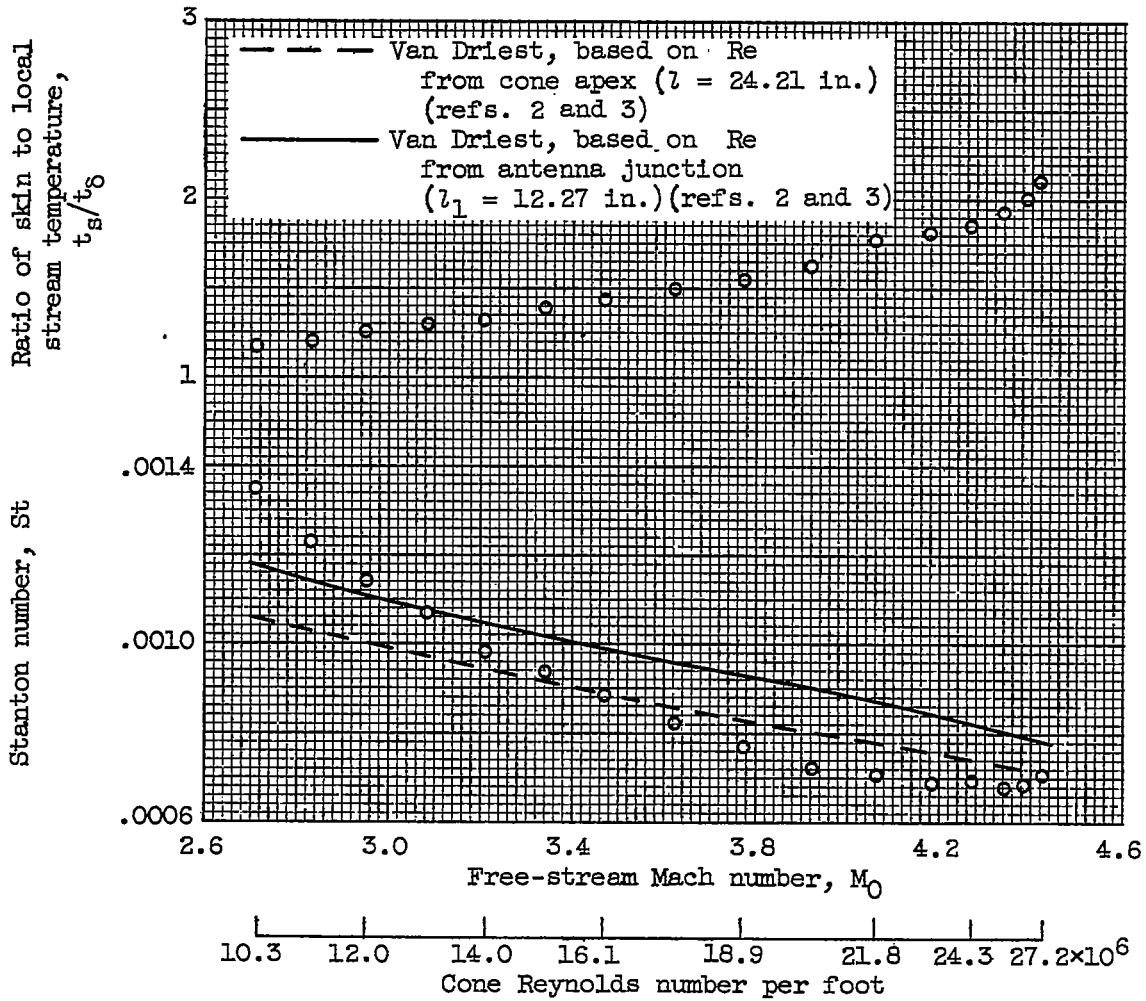
(d) Slant distance from cone apex, 22.34 inches.

Figure 15. - Continued. Ratio of skin to local stream temperature and Stanton number against free-stream Mach number and cone Reynolds number per foot for model 3.

~~CONFIDENTIAL~~

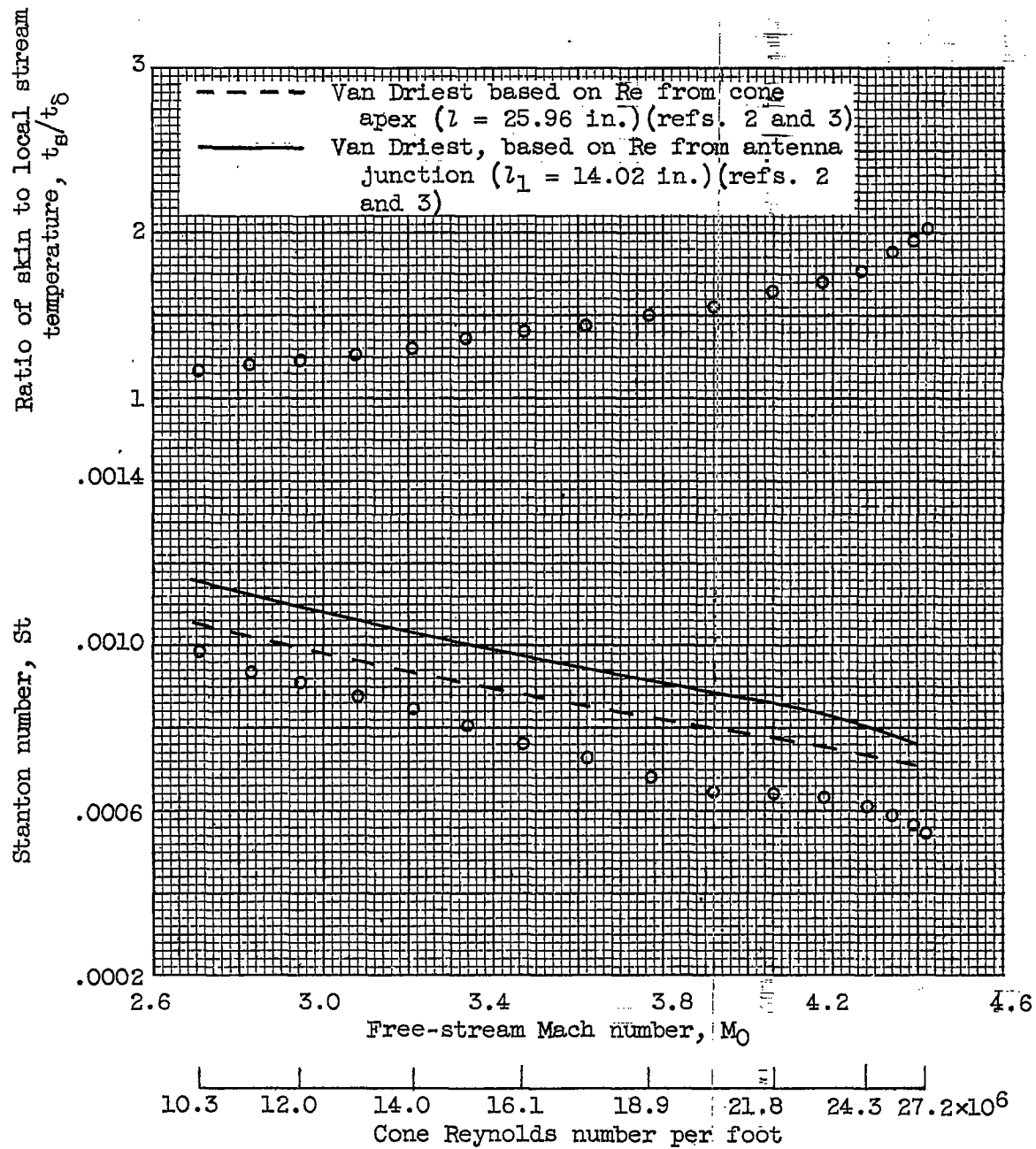
3661

CF-7



(e) Slant distance from cone apex, 24.21 inches.

Figure 15. - Continued. Ratio of skin to local stream temperature and Stanton number against free-stream Mach number and cone Reynolds number per foot for model 3.

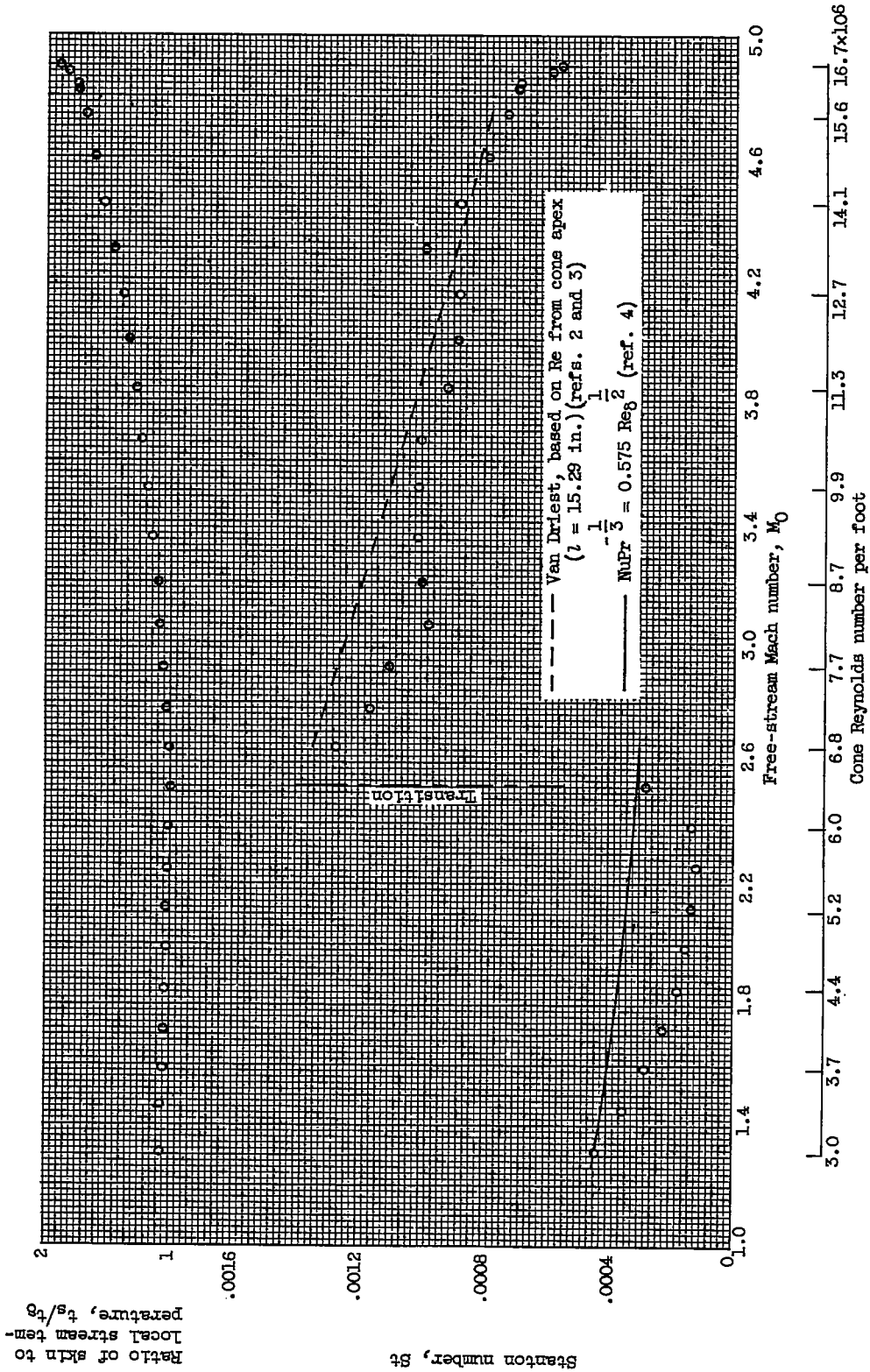


(f) Slant distance from cone apex, 25.96 inches.

Figure 15. - Concluded. Ratio of skin to local stream temperature and Stanton number against free-stream Mach number and cone Reynolds number per foot for model 3.

3661

CE-7 back

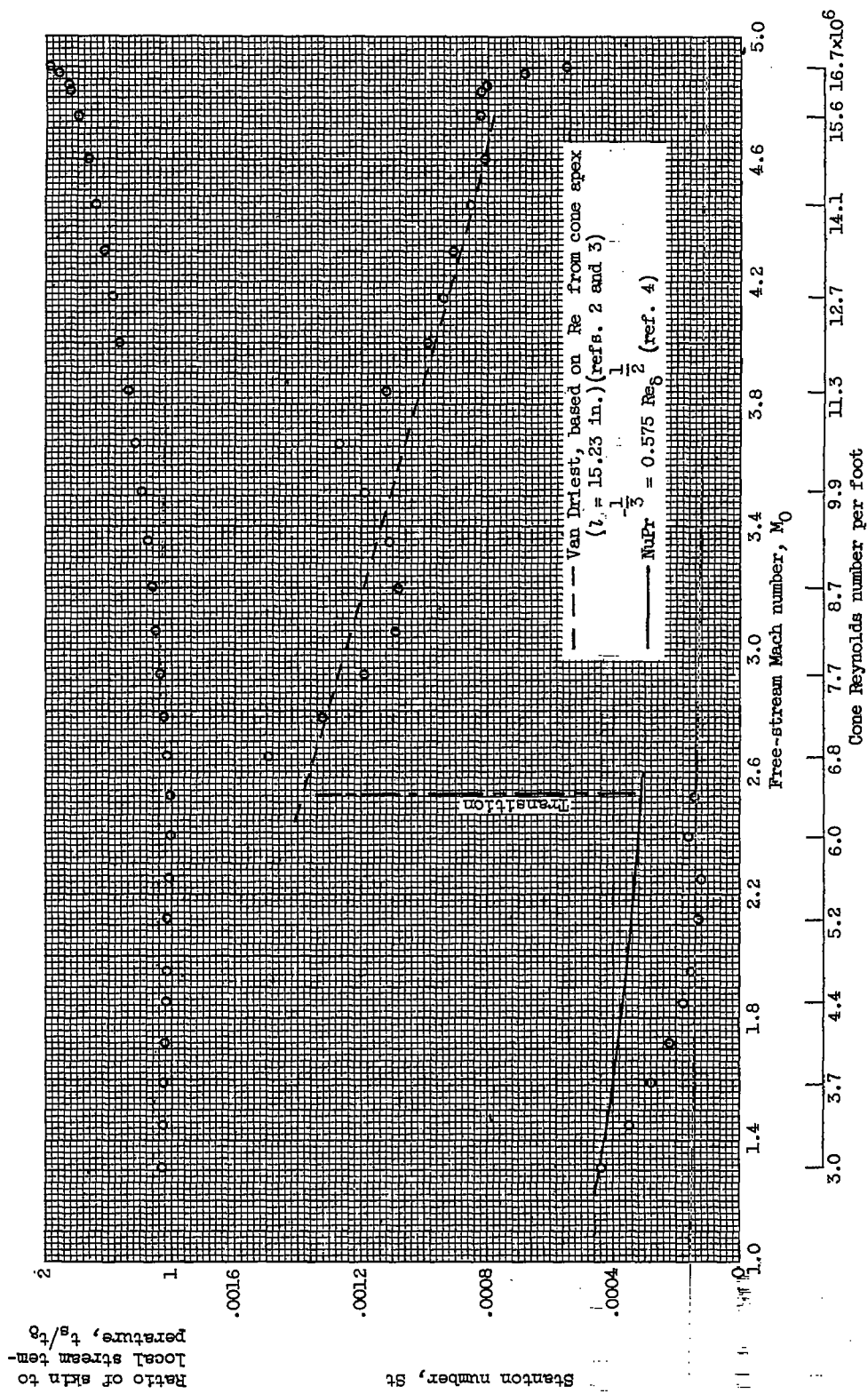


(a) Slant distance from cone apex, 15.29 inches.

Figure 16. - Ratio of skin to local stream temperature and Stanton number against free-stream Mach number and cone Reynolds number per foot for model 4.

CONFIDENTIAL

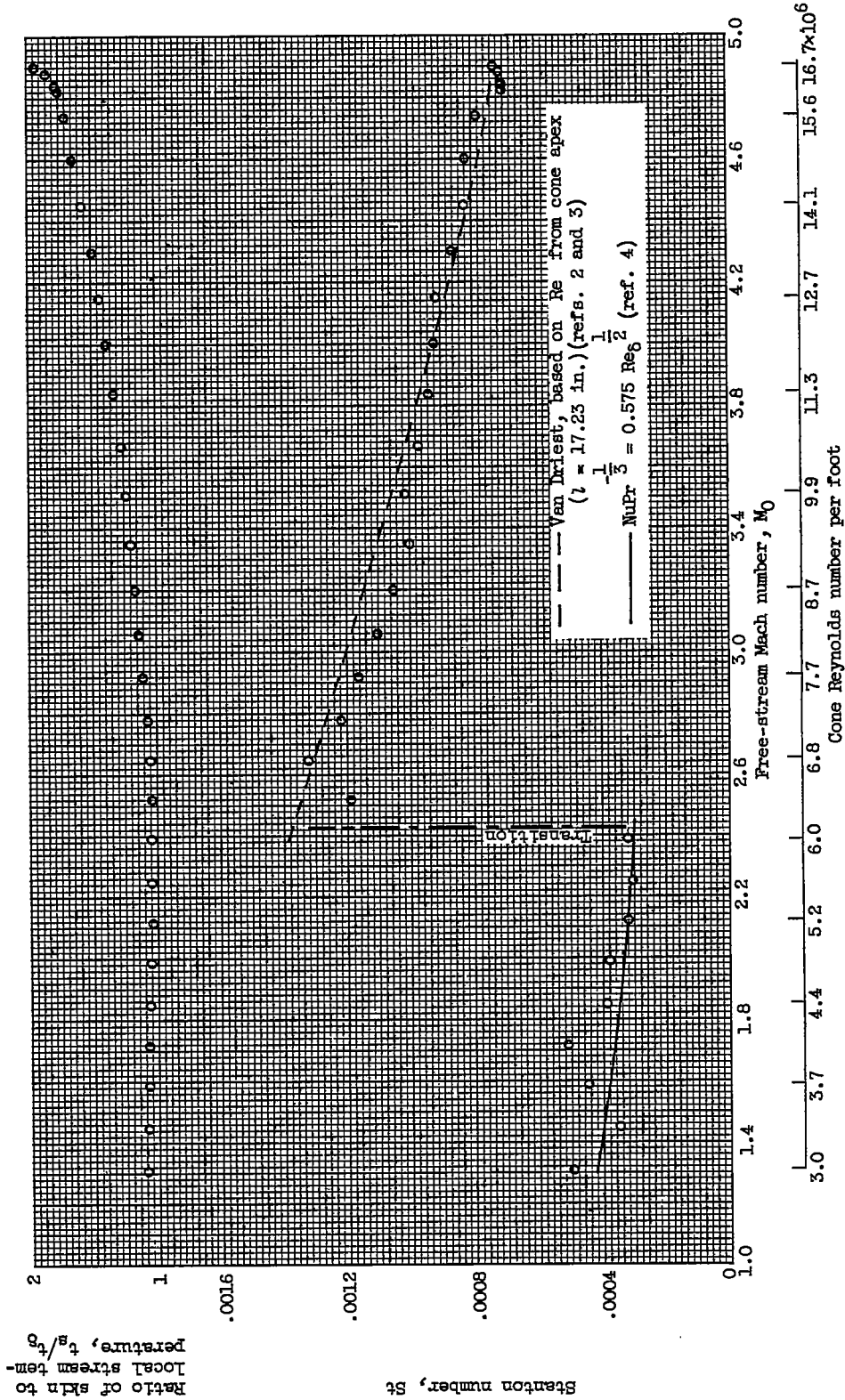
NACA RM E55F27



(b) Slant distance from cone apex, 15.23 inches.

Figure 16. - Continued. Ratio of skin to local stream temperature and Stanton number against free-stream Mach number and cone Reynolds number per foot for model 4.

3661

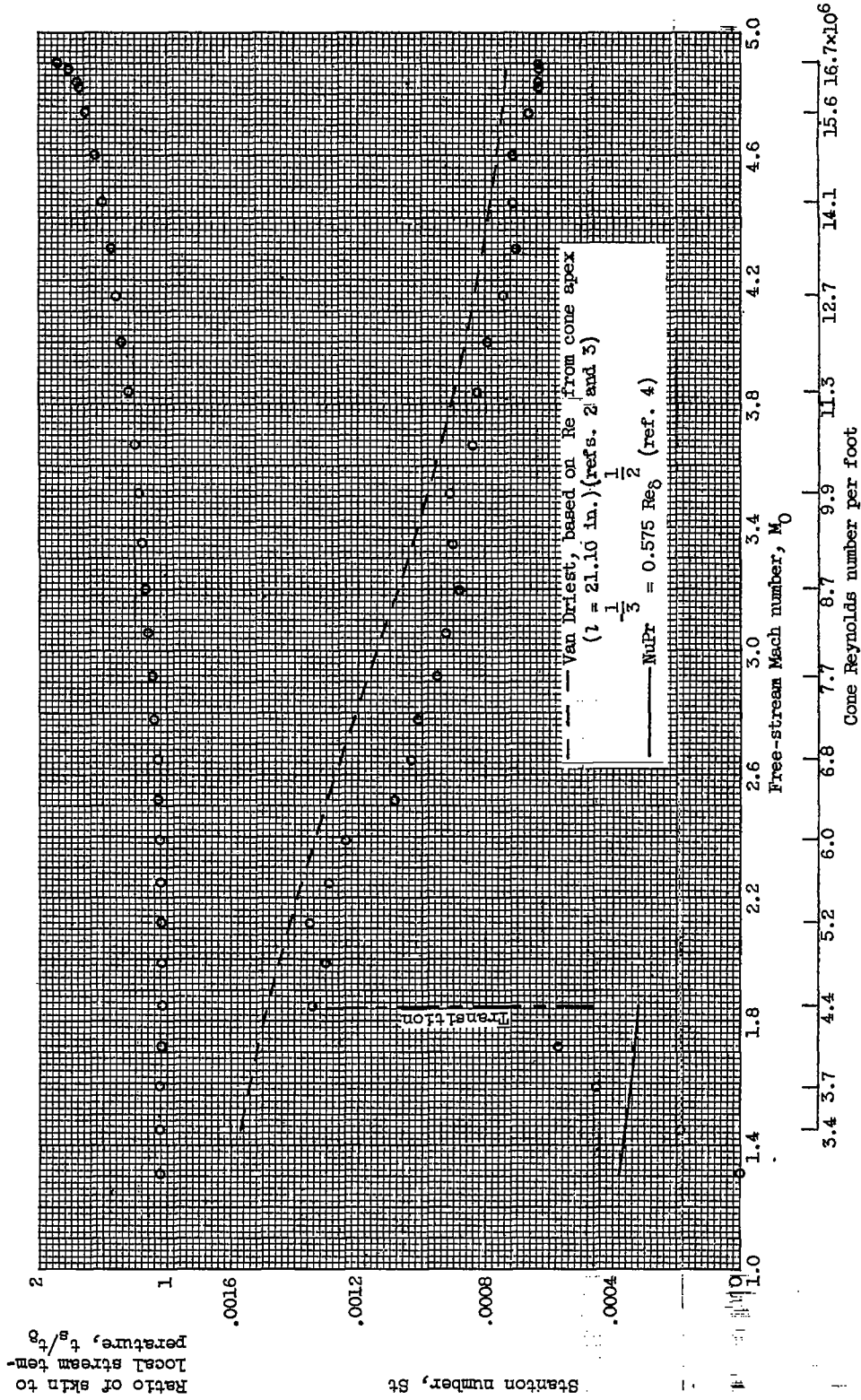


(c) Slant distance from cone apex, 17.23 inches.

Figure 16. - Continued. Ratio of skin to local stream temperature and Stanton number against free-stream Mach number and cone Reynolds number per foot for model 4.

~~CONFIDENTIAL~~

NACA RM E55F27

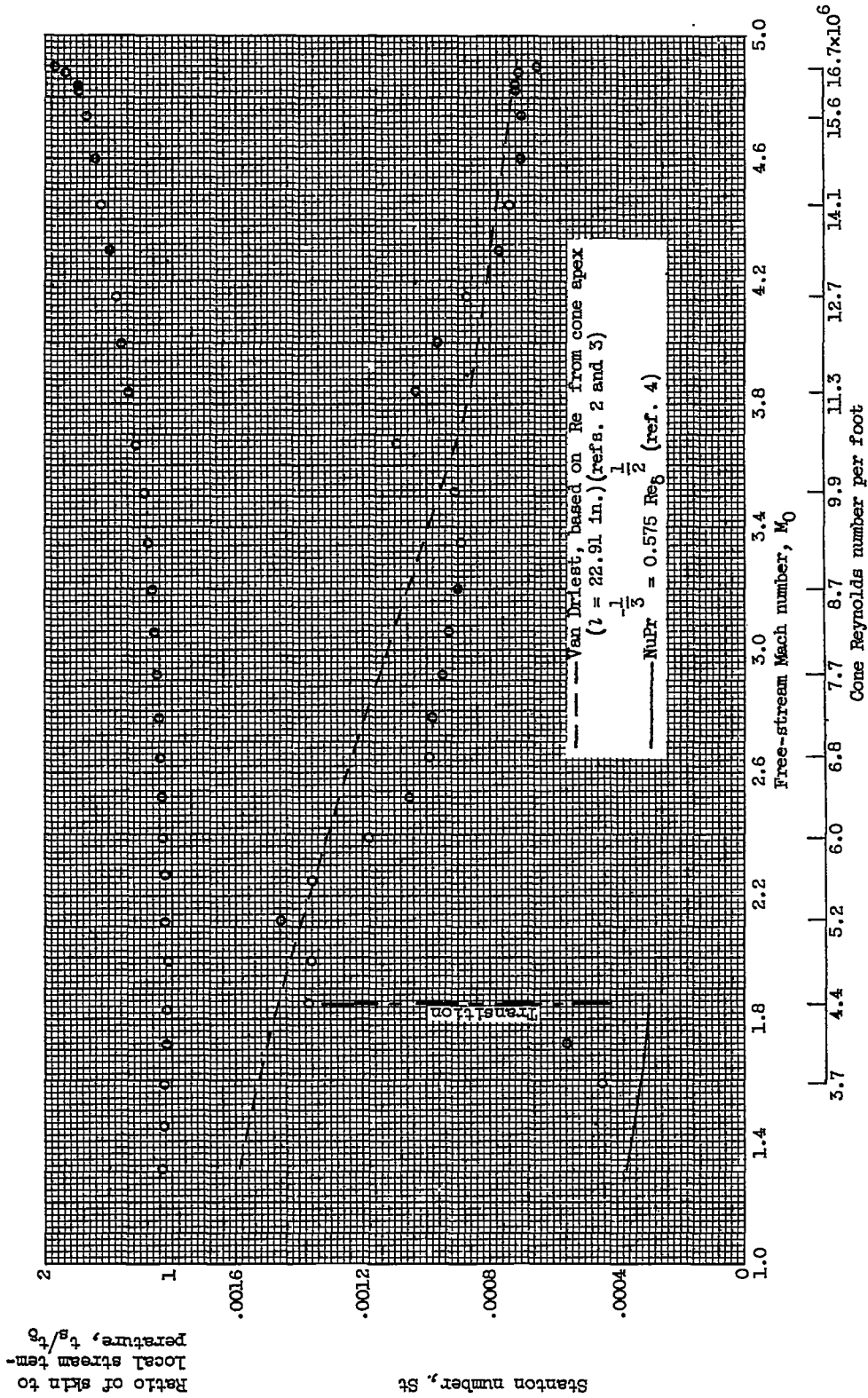


(d) Slant distance from cone apex, 21.10 inches.

Figure 16. - Continued. Ratio of skin to local stream temperature and Stanton number against free-stream Mach number and cone Reynolds number per foot for model 4.

~~CONFIDENTIAL~~

Job 1



(e) Slant distance from cone apex, 22.91 inches.

Figure 16. - Concluded. Ratio of skin to local stream temperature and Stanton number against free-stream Mach number and cone Reynolds number per foot for model 4.

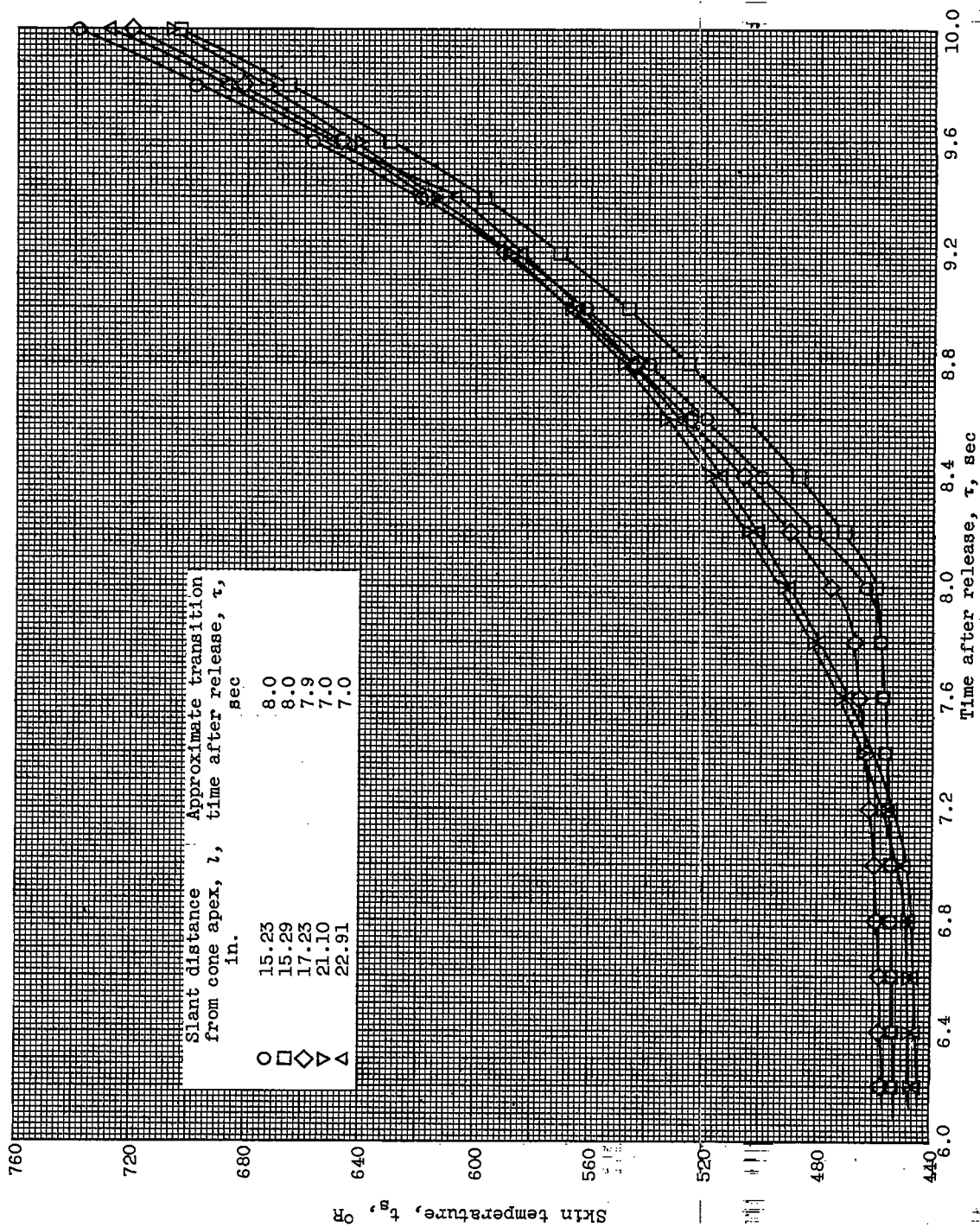


Figure 17. - Time history of measured skin temperatures during boundary-layer transition for model 4.

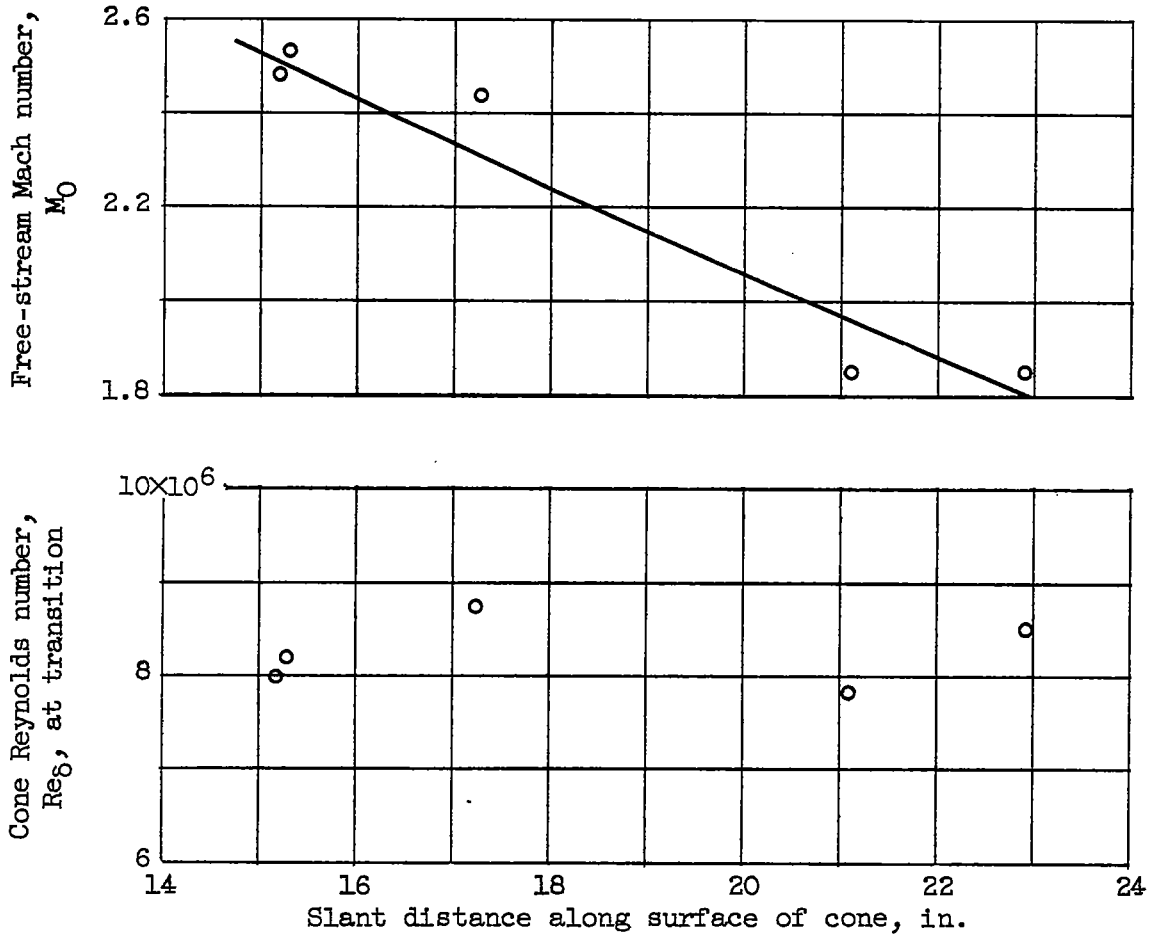


Figure 18. - Transition Reynolds number and corresponding free-stream Mach number for each temperature measuring station (model 4).

CONFIDENTIAL

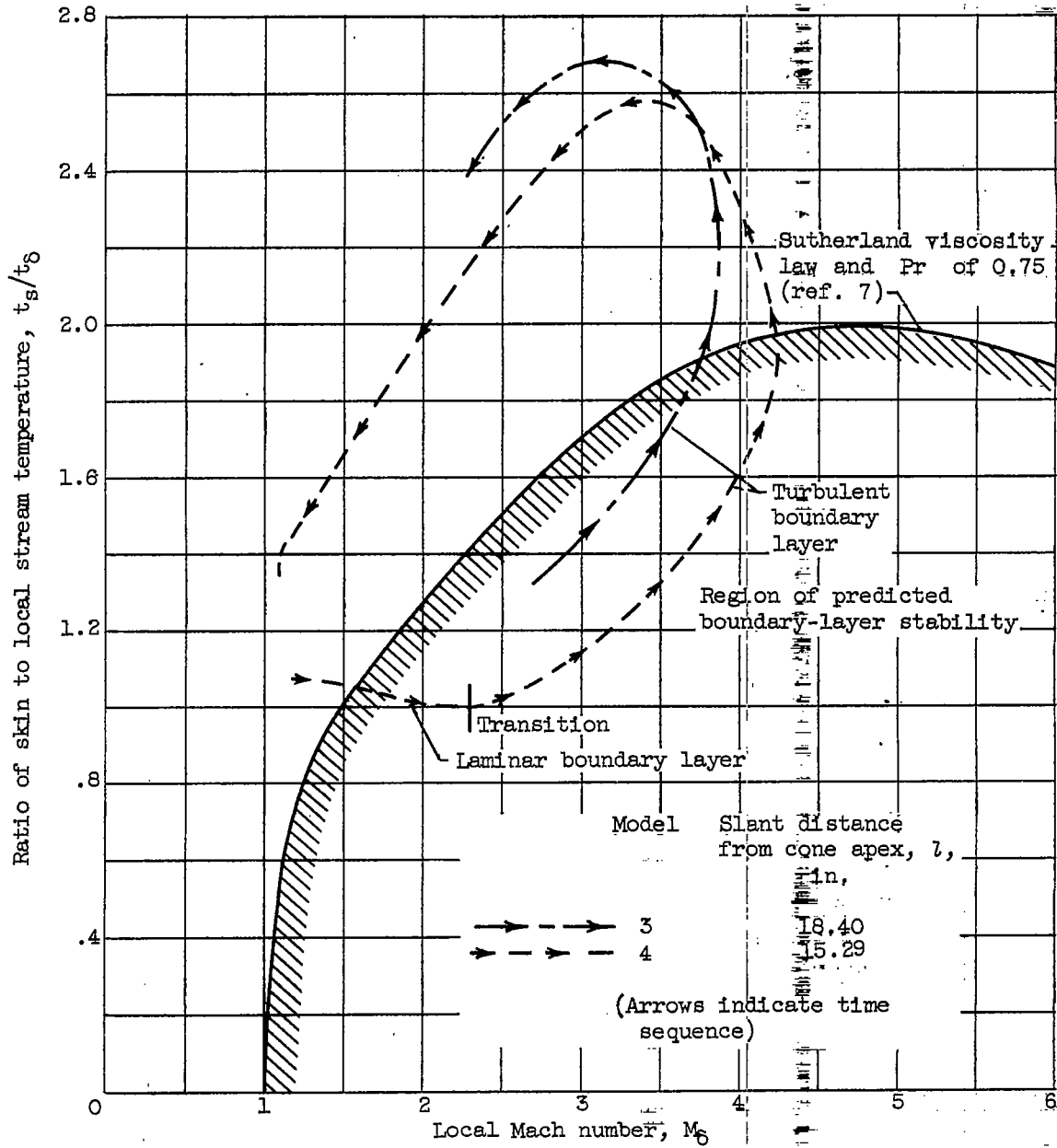


Figure 19. - Skin-temperature ratio against local Mach number for typical stations on models 3 and 4.

CONFIDENTIAL